Multi-omics investigation of spontaneous T2DM macaque reveals gut microbiota promote T2DM by up-regulating the absorption of excess palmitic acid

Xu Liu[1], Shengzhi Yang[1], Yuchen Xie[1], Cong Jiang[1], Ke Shang[1], Jinxia Luo[1,3], Lin Zhang[1], Gang Hu[2], Qinghua Liu[2], Bisong Yue[1], Zhenxin Fan[1], Zhanlong He[4], Jing Li[1*]

[1] Key Laboratory of Bio-resources and Eco-environment (Ministry of Education), College of Life Sciences, Sichuan University, Chengdu 610065, China.

[2] SCU-SGHB Joint Laboratory on Non-human Primates Research, Meishan, Sichuan, China.

[3] Sichuan Key Laboratory of Development and Application of Monkey Models for Human Major Disease, Sichuan, China.

[4] Institute of Medical Biology, Chinese Academy of Medical Sciences and Peking Union Medical College, Yunnan, China.

* Correspondence:

Jing Li (ljtjf@126.com)

College of Life Sciences, Sichuan University

Abstract

Although gut microbiota and lipid metabolites have been suggested to be closely associated with type 2 diabetes mellitus (T2DM), the interactions between gut microbiota, lipid metabolites and the host in T2DM development remains unclear. Rhesus macaques may be the best animal model to investigate these relationships given their spontaneous development of T2DM. We identified eight spontaneous T2DM macaques and conducted a comprehensive study investigating the relationships using multi-omics sequencing technology. Our results from 16S rRNA, metagenome, metabolome and transcriptome analyses identified that gut microbiota imbalance, tryptophan metabolism and fatty acid β oxidation disorders, long-chain fatty acid (LCFA) accumulation, and inflammation occurred in T2DM macaques. We verified the accumulation of palmitic acid (PA) and activation of inflammation in T2DM macaques. Importantly, mice transplanted with spontaneous T2DM macaque fecal microbiota and fed a high PA diet developed prediabetes within 120 days. We determined that gut microbiota mediated the absorption of excess PA in the ileum, resulting in the accumulation of PA in the serum consequently leading to T2DM in mice. In particular, we demonstrated that the specific microbiota composition was probably involved in the process. This study provides new insight into interactions between microbiota and metabolites and confirms causative effect of gut microbiota on T2DM development.

Key words: spontaneous T2DM macaques, multi-omics, gut microbiota, palmitic acid, fecal microbiota transplantation

Introduction

Diabetes mellitus is considered to be a refractory disease causing a significant socio-economic burden. Type 2 diabetes mellitus (T2DM) is the dominant type of diabetes mellitus characterized by metabolic disorders, insulin resistance, and deficiency of insulin secretion (1, 2). The pathogenesis of this chronic disease is complex and genetic and environmental factors, such as sugar and lipid intake, gut microbiota, many metabolites, and even air pollutants, contribute to its increase in prevalence (3, 4). Accumulating evidence has linked gut microbiota with T2DM development by variety ways. The gut microbiota can impact the integrity of the intestinal epithelial barrier, mediate insulin resistance, as well as regulate the function of mitochondria (5, 6, 7). They can regulate local or systemic immunity and inflammation, which also contributes to the development of T2DM (8). Moreover, various gut microbial metabolites, such as short-chain fatty acids, bile acid, and tryptophan-derived metabolites, have been reported to be closely related to the pathogenesis of T2DM (5, 6, 9, 10). However, the interactions between gut microbiota and its host with T2DM have not yet been fully characterized. In pathological conditions, the dysregulation of the host can lead to changes in gut microbiota composition. In turn, the microbiota plays a regulatory role to participate in the development of T2DM. Despite the complicate interactions between host and microbiota in the context of T2DM, some studies suggest antidiabetic interventions targeting the gut microbiota such as fecal microbiota transplanting (FMT) can be applied as a clinical treatment of T2DM (11, 12, 13).

Meanwhile, dysfunction of lipid metabolism contributes to T2DM development by inducing lipotoxicity in humans and animal models (14, 15). The long-chain fatty acids (LCFAs) are the principal lipid components naturally occurring in animal fats and vegetable oil, as well as the main metabolites of fat. LCFAs such as palmitic acid (PA, C16:0), palmitoleic acid (C16:1N7), and oleic acid (C18:1N9), are reported to have strong association with T2DM. In the last few decades, there is increasing

evidence that frequent consumption of LCFAs contributes to metabolic diseases such as obesity and T2DM due to the high PA content (16, 17). PA is a saturated fatty acid and its increase in serum is a significant contributing factor in T2DM development (18, 19, 20). The suggested mechanisms by which PA mediates T2DM include increasing diacylglycerol and ceramide synthesis (21), mitochondrial and endoplasmic reticulum stress (22, 23), and activation of pro-inflammatory pathways (24). Nevertheless, whether gut microbiota involving in PA mediated T2DM and the interactions between gut microbiota and LCFA metabolites in T2DM development are still unclear.

Spontaneous development of T2DM in non-human primates (e.g. macaques) is highly similar to human T2DM, such as insulin resistance in early stages and later abnormal glucose tolerance and T2DM development follows the same pathological changes of pancreatic islets and complications. In fact, T2DM macaques and humans have amyloidosis of pancreatic islets but it is not observed in mouse models (25, 26), suggesting that T2DM macaques are the best animal model that can simulate and reproduce human T2DM and its complications (27). However, previous studies indicated that naturally occurring spontaneous T2DM macaques in captive populations were rare even if individuals were given a high lipid and high sugar diet (28, 29). After nasally fed cynomolgus macaques with a high-fat dietary emulsion for 12 months, the macaques did not experience significant increases in fasting blood glucose and glycosylated hemoglobin (29). The controversial effects of high fat on the T2DM development are worthy of further investigations to better understand this complex disease.

Here, this study identified spontaneous development of T2DM in individuals (hereafter spontaneous T2DM macaques) from a large group of rhesus macaques. These spontaneous T2DM macaques have never been treated with anti-diabetic drugs and therefore provide valuable models for pathogenesis investigation of T2DM. Based on the macaque model, we used multi-omics techniques to address the interactions between gut microbiota, host gene expression, and fecal metabolites and

the development of T2DM. Our results demonstrated that gut microbiota and LCFA metabolites played important roles in the pathogenesis of T2DM. We validated the increased content of plasma PA and activation of inflammation in the T2DM macaques. In addition, we successfully induced prediabetes in mice by transplanting fecal microbiota from T2DM macaques into mice in conjunction with a diet high in PA. We also revealed the specific structure of gut microbiota that promoted T2DM development by regulating the absorption of excess PA, which provides key evidence of the causative effect of gut microbiota on the pathogenesis of T2DM.

Results

Metagenome and 16S sequencing demonstrate alterations on gut microbiota in spontaneous T2DM macaques

We identified eight spontaneous T2DM macaques out of 1698 individuals from long-term glucose monitoring in a captive population (Table S1). The fasting plasma glucose (FPG), fasting plasma insulin (FPI), and HOMA-IR levels in the T2DM macaques were significantly higher than in the control group ($p<0.01$), suggesting insulin resistance in T2DM macaques. However, glycosylated hemoglobin A1c (HbA1c), triglycerides (TG), total cholesterol (TC), high-density lipoprotein cholesterol (HDL), low-density lipoprotein cholesterol (LDL), and BMI did not significantly differ from the controls ($p>0.05$, Table 1). Comparison of gut microbiota between the two groups based on 16S rRNA amplicon found that both Shannon and Simpson index decreased in T2DM macaques but it was not significantly different from controls ($p>0.05$; Figures 1A and B). PCoA indicated that the microbiota composition of spontaneous T2DM macaques was different from the control group (Figure 1C). As one of the most dominant families in both groups, Lachnospiraceae showed significantly higher abundance in the T2DM group (14.48%) than in the control group (6.66%). While the abundance of the Lactobacillaceae family was significantly greater in the control group (25.95%) compared to spontaneous T2DM macaques (20.88%) (Figure 1D). A total of 21 microbes were identified as

differentially microbes between the T2DM group and control group, where ten microbes including Erysipelotrichaceae and five members in Lachnospiraceae family (*Ruminococcus gnavus*, *Lachnospira*, *Coprococcus* sp. *Dorea longicatena*, and *Roseburia*) were significantly greater in the T2DM group (Figure 1E).

The metagenome results showed that the T2DM group had a higher abundance of Erysipelorictchaeae, *Eubacterium rectale*, Lachnospiraceae, Negativicutes, *Blautia*, and Coriobacteriia than the control group (Figure S1A). Functional enrichment demonstrated a total of 74 KEGG pathways with significant differences between the two groups. These pathways were mainly associated with T2DM and inflammation, including type II diabetes mellitus, glucagon signaling pathway, starch and sucrose metabolism, lipid metabolism, and toll-like receptor signaling pathways (Figure 1F). Among the six CAZy enzyme families, the Carbohydrate-binding module (CBMs), Glycosyl Transferases (GTs), Carbohydrate esterases (CEs), and Polysaccharide Lyases (PLs) families were significantly upregulated in the T2DM group, indicating significant changes in carbohydrate metabolism (Figure 1G). The results of metagenome and 16S sequencing demonstrated significant alterations in the composition and function of gut microbiota in spontaneous T2DM macaques, with a greater abundance of microbes associated with T2DM and fewer beneficial microbes.

Fecal metabolome and blood transcriptome reveals dysfunction of fatty acid β oxidation and tryptophan metabolism in T2DM macaques

The UHPLC-MS based metabolome analysis on fecal samples of T2DM and control macaques identified 1564 metabolites belonging to various types of secondary metabolites, with lipids and lipid-like molecules being most abundant (31.1%) (Figure S1B). We found 64 significantly differential metabolites between the two groups using a combined multidimensional statistical analysis (OPLS-DA) and univariate statistical analysis (T-test) (VIP>1, $p<0.05$) (Figures 2A and B; Table S2). Among them, muscon, indole-3-acetaldehyde, and serotonin were significantly lower in the

T2DM group (Figure 2C) and are associated with anti-inflammatory activity (30, 31, 32). Notably, 64 differential metabolites were significantly enriched in one pathway: tryptophan metabolism (Figure 2D), and we identified two significantly different metabolites, indole-3-acetaldehyde and serotonin in this pathway. Both metabolites are microbiota-derived tryptophan metabolites and the ligands for AhR (31, 32). The lower concentration of AhR ligands may lead to the development of inflammation and metabolic syndromes in humans (33). In addition, we found the contents of many acylcarnitine metabolites were significantly higher in the T2DM group (VIP>1, $p<0.1$), including l-propionylcarnitine, hexanoyl-l-carnitine, (r)-butyrylcarnitine, and isovaleryl-l-carnitine (Table S2). Among them, l-propionylcarnitine, a kind of acylcarnitines, was the most upregulated metabolite in the T2DM macaques (FC: 16.19) (Figure 2C). Acylcarnitines are products of incomplete oxidation of LCFAs, which can activate pro-inflammatory signaling pathways and ultimately inhibit insulin activity (34). Our results indicated incomplete LCFAs β oxidation in spontaneous T2DM macaques, while similar characteristics were also observed in insulin resistant and T2DM humans (35, 36).

Blood transcriptome analysis was consistent with metabolome results, indicating dysfunction of fatty acid β oxidation and inflammation in T2DM macaques. Gene expression in T2DM macaques exhibited significant differences from the controls (Figure 2E), and a total of 161 differentially expressed genes (DEGs) (26 upregulated and 135 downregulated) were identified in T2DM macaques at a FDR level of 0.05 (Figure 2F). Enrichment analysis of the DEGs was linked to diabetes, fatty acid metabolism, and inflammation, such as diabetic cardiomyopathy, glucose homeostasis, fatty acid metabolic process, and chemokine production (Figure 2G). We also identified 26 differential enrichment pathways between the two groups by aggregate fold change (AFC), and most were associated with insulin resistance and inflammation, including insulin resistance, PI3K-Akt signaling pathway, bacterial invasion of epithelial cells, and NOD-like receptor signaling pathway (Figure S2A). As shown in the insulin resistance pathway, expression of *IL6* and *IRS1* were

upregulated, while *INSR* was downregulated in T2DM macaques (Figure S2B). The WGCNA analysis identified four modules that were related to T2DM. Darkgreen module and brown module were significantly positively correlated with T2DM, while green module and darkred module were negatively correlated with T2DM (Figure 2H). Genes in the darkgreen module and brown module related to lipolysis and inflammation were significantly upregulated in T2DM macaques, and genes in the green module and darkred module related to fatty acid metabolism and insulin secretion were significantly downregulated (Figure S2C). With the cut-off (|kME>0.8|), a total of 546 genes in the four modules were identified as hub genes (Table S3). Of these 546, 102 hub genes were also DEGs (Figure 2I). Several of these genes have been reported as correlated with T2DM in humans, including *IGF2BP2*, *LEPR*, *RAP1A*, *SESTRIN 3*, and *ITLN1* (37, 38, 39, 40, 41). In addition, *ACSM3*, *HADHB*, and *EFHB* are involved in fatty acid β oxidation and inflammation (42, 43, 44).

Validation of LCFAs accumulation and inflammation in T2DM macaques

Collectively, metabolome and transcriptome results indicated dysfunction in fatty acid β oxidation and tryptophan metabolism in T2DM macaques, which may lead to LCFA accumulation and inflammation. To support this conclusion, we performed targeted medium-and long-chain fatty acid mass spectrometry of plasma and examined serum inflammatory cytokines in the macaques. A total of 34 fatty acids were detected, and among the five types of fatty acids, the concentration of saturated fatty acid (SFA) was significantly greater in the T2DM group (p<0.05, Figure 3A), while other types of fatty acids were not significantly different between the two groups (p>0.05, Figures 3B-E). In particular, concentrations of PA, palmitoleic acid, and oleic acid were significantly higher in the T2DM group than control group (p<0.05 and VIP>1, Figures 3F and G). Increased content of PA, palmitoleic acid, and oleic acid was also found in human T2DM (45, 46). PA was an important metabolite mediating insulin

resistance through three main mechanisms, being increased diacylglycerol and ceramide synthesis, mitochondrial and endoplasmic reticulum stress, and activation of pro-inflammatory pathways through membrane receptors (21, 22, 23, 24). Analysis on the serum inflammatory cytokines found that IL-1β was significantly higher in the T2DM group (p<0.05, Figure 3H), but TNF-α and IL-6 levels showed no significant difference between the two groups (p>0.05, Figures 3I and J). IL-1β is a major player in a variety of autoinflammatory diseases and a key promoter of T2DM systemic and tissue inflammation (47). Moreover, blood routine examination showed an increase of WBC number, NEU percentage and NEU number and a decrease of LYM percentage and LYM number, also indicating the inflammation in the T2DM macaques (p<0.05, Table 2).

To investigate effect of gut microbiota on the LCFAs accumulation and inflammation in T2DM macaques, we performed a correlation analysis among the DEGs, differential metabolites, and differential microbes using spearman rank correlation. Four differential microbes in Lachnospiraceae family (*Coprococcus*, *Lachnospira*, *Roseburia* and *Dorea longicatena*) were significantly associated with three differential metabolites of PA, palmitoleic acid and oleic acid (|r|>0.5, adj p<0.05), suggesting the participation of Lachnospiraceae microbes in LCFAs accumulation in T2DM macaques (Figure 3K). In addition, the bacteria in class Coriobacteriia was also associated with the three LCFAs (|r|>0.5, adj p<0.05, Figures S1C and D).

Fecal microbiota transplantation (FMT) with high content PA food induce prediabetes in mice

To determine the causative effect of gut microbiota and PA on T2DM development, we collected feces from the spontaneous T2DM macaques and performed fecal microbiota transplantation (FMT) in antibiotic-pretreated mice. Mice were either administrated by FMT (FT), fed with high concentration PA diet (PA), or were combined FMT and PA diet (FTPA). A control group was used and they were fed with

normal commercial food and lacked FMT (Figure 4A). FPG monitoring found that FPG levels in the FTPA group and FT group increased continuously from day 60 (Figure 4B), while the control group maintained stable FPG levels throughout the 120 days. The FTPA group showed the highest FPG of 6.7 mmol/L at day 120, which was significantly higher than the control group and indicated FTPA-treated mice had developed prediabetes (Figure 4C). The oral glucose tolerance test (OGTT) showed obvious glucose intolerance in the FTPA group (Figures 4D and E), and the FPI values and insulin tolerance test (ITT) were both significantly elevated in the FTPA group, indicating insulin resistance (Figures 4F and G). Meanwhile, body weight (BW), TC, and TG significantly increased in the FTPA group (Figures 4H-J). While mice in the FT group and PA group had significant weight gain and mild insulin resistance, they did not exhibit significant glucose intolerance and no significant elevation in TC and TG levels compared to controls. Histopathological changes in the pancreas and liver of mice were investigated using H-E staining. Hepatocytes focal necrosis with inflammatory cell infiltration was commonly observed in the FTPA mice, but not frequent in hepatocytes in FT and PA groups (Figure 4K). Furthermore, decreased volume and area in pancreatic islets and inflammatory cell infiltration were detected in the FTPA mice (Figure 4L), while such pathological changes were not found in the control group.

Specific structure of gut microbiota mediates the absorption of excess PA in the ileum

Given that the content of plasma PA significantly increased in the T2DM macaques (Figures 3F and G), we examined PA content in the feces, ileum, and serum in mice to compare the prediabetes mice and the spontaneous T2DM macaques. PA content in the serum and ileum of the FTPA group was significantly higher than the control group ($p<0.05$, Figures 5A and B), but its content in feces was significantly lower than the control group ($p<0.05$, Figure 5C). This suggested that the absorption of PA was significantly enhanced in the ileum leading to the increase of PA in serum. To

verify this conclusion, expression of the *Cd36* gene, a gene involved in the uptake and oxidation of LCFAs (48), was examined in the ileum of mice. Ileums showed a significantly upregulated expression of *Cd36* in the FTPA group compared to the control group ($p<0.05$, Figure 5D). In contrast, the level of IL-17A, a protein inhibiting the expression of *Cd36* (49), was significantly reduced in the ileum of the FTPA group ($p<0.05$, Figure 5E). Interestingly, the PA group's content of PA, *Cd36* expression and IL-17A was not significantly different from the control group. This indicated that without FMT, the ileum could not absorb PA effectively even when fed in high concentrations. Consequently, gut microbiota mediated the absorption of excess PA in the ileum.

We then compared diversity and composition of microbiota communities between the FTPA, FT, PA and control groups, and a fifth group consisting of the microbiota transplants (TP) from T2DM macaques. Shannon and Simpson indices were lower in the FTPA, FT and PA groups than the control group (Figures S3A and B). NMDS analysis also indicated a distinct microbiota composition from the control group compared to other groups (NMDS1). In addition, microbiota composition of TP from T2DM macaques was distinct from other groups but a little closer to the FTPA and FT groups (NMDS2, Figure 5F). In particular, the Lachnospiraceae family showed the higher abundance in the TP, FTPA and FT groups than in the PA and control groups (Figure S3C). The abundances of three members of microbes in Lachnospiraceae (*R. gnavus* and *Coprococcus* sp. and *Clostridium*) in the FTPA and FT groups gradually increased over time after FMT (Figure S3D). The FTPA and FT groups shared many differential microbes compared to the control group, such as the significantly upregulated *R. gnavus* and *Coprococcus* sp., and the significantly downregulated Christensenellaceae, F16, *Treponema* sp. and *Fibrobacter succinogenes* (Figures 5G and H). It is noteworthy that these microbes were also differential microbes between T2DM macaques and controls, and their abundances changed in the same way as in macaques (Figure 1E). However, mice in the PA group did not share differential microbes with the spontaneous T2DM macaques.

Correspondingly, the change of serum PA content in the PA group was not significantly higher than the control group (Figure S3E). Our results suggested that the transplanted microbiota from spontaneous T2DM macaques, especially the increased abundance of *R. gnavus* and *Coprococcus* sp. and decreased abundance of *Treponema*, *F. succinogenes*, Christensenellaceae and F16, promoted the absorption of excess PA by regulating the expression of IL-17A and Cd36, leading to the LCFAs accumulation and insulin resistance (Figures 5I).

Discussion

With a multi-omics technology, this study comprehensively characterizes the gut microbiota, metabolites and gene expression of spontaneous T2DM macaques. The gut microbiota diversity in T2DM macaques decreased. In particular, the abundance of bacteria *R. gnavus* and Erysipelotrichaceae were upregulated while the abundance of Christensenellaceae was downregulated in the T2DM macaques. Metabolome results demonstrated a decrease of microbiota-derived tryptophan and anti-inflammatory metabolites, indicating that T2DM macaques were prone to inflammation. Notably, the accumulation of acylcarnitine metabolites, the suggested biomarkers for human T2DM (46), indicated incomplete mitochondrial LCFA β oxidation in T2DM macaques. Transcriptome results identified many DEGs linked to insulin resistance, fatty acid β oxidation and inflammation, including *IGF2BP2*, *LEPR*, *RAP1A*, *SESTRIN 3*, and *ITLN1* that have also been reported in human T2DM (37, 38, 39, 40, 41). Combining the multi-omics results we revealed the complex pathological mechanisms in the spontaneous T2DM macaques (Figure 6), which is comparable to T2DM humans. Firstly, expression of genes related to lipolysis, fatty acid oxidation, LCFA accumulation, inflammation, and insulin seretion are dysregulated, promoting the development of T2DM (Figure 6A). This is particularly related to lipid metabolism, where the increase of lipolysis and the downregulated expression of fatty acid metabolism-related genes *HADHB* and *ACSM3* cause the accumulation of acylcarnitine and LCFAs, which results in incomplete LCFA oxidation in T2DM macaques (Figure 6B). We also suggest that the decrease of *Lactobacillus* sp. cause

the reduction of Aryl hydrocarbon receptor (AhR) ligands (serotonin and indole-3-acetaldehyde) given that *Lactobacillus* is producer of AhR ligands (50). This then promotes the expansion of the PA producer Erysipelotrichacea (51, 52) and ultimately leads to the increase of PA levels. The increase in the abundance of Erysipelotrichacea and *R. gnavus* also promotes the development of T2DM by activation of inflammation (53, 54, 55) (Figure 6C). The accumulation of PA was reported to lead to insulin resistance by affecting genes in the insulin signaling pathway (16). Our study demonstrates that the significantly changed expression of *RAP1A*, *SESTRIN3*, and *IRS1* in PA-mTORC1-Akt pathway causes insulin resistance in T2DM macaques. Moreover, the increase of PA can promote the development of T2DM by upregulating the NF-κB signaling pathway (Figure 6D).

We validated the observations from the multi-omics analysis finding the significantly higher inflammatory cytokines IL-1β and LCFA accumulation, especially significant PA accumulation in the T2DM macaques. And found LCFA metabolites were significantly correlated with bacteria in the Lachnospiraceae family. Numerous studies imply an association of gut microbiota with T2DM development. By transplanting gut microbiota from healthy individuals to T2DM individuals, symptoms such as insulin resistance or inflammation were improved (6, 56). However, there is no evidence to date suggesting gut microbiota have directly causative effects on T2DM development. Our study confirmed the causative effect of gut microbiota and PA on T2DM development by transplanting fecal microbiota from spontaneous T2DM macaques to antibiotic pretreated mice. We successfully induced prediabetes in mice after combining FMT administration and high PA ingestion. However, when the treatments were administered on their own, the mice did not develop prediabetes. We determined, for the first time, that gut microbiota mediated the absorption of excess PA in the ileum by quantitative examining PA contents in feces, ileum, and serum, and analysis of the expression of *Cd36* and IL-17A level in the ileum. Most notably, this then resulted in accumulation of PA in the serum and finally led to T2DM development. Without the transplanting gut microbiota, the ileum could not absorb the

PA effectively even at a high concentration of ingested PA. Our study highlights the essential roles of gut microbiota in T2DM development, and this is probable also the reason that previous studies have failed to induce T2DM in macaques because they have only used a high-fat diet (28, 29).

We then determined the specific gut microbiota structure that related to T2DM development in the prediabetes mice and spontaneous T2DM macaques. We found that the increased abundance of *R. gnavus* and *Coprococcus* sp., and the decreased abundance of *Treponema*, *F. succinogenes*, Christensenellaceae, and F16, were involved in the T2DM development. *R. gnavus* can promote insulin resistance by regulating the content of tryptamine/phenethylamine (57). Moreover, *R. gnavus* is a mucin-degrading microbe that leads to an increase of inflammation (58, 59, 60). The intestinal mucous layer is an important barrier separating intestinal tissue from microbiota, and microbiota composition plays a major role in affecting the integrity of intestinal mucous layer (58). The increase of *R. gnavus* suggested a higher risk of damage to the integrity of the intestinal mucous layer. This is further supported by our results of the lower abundance of *Lactobacillus* sp., which are AhR ligand producers, and the decreased content of AhR ligands (tryptophan microbial metabolites) in spontaneous T2DM macaques. The deficiency of AhR ligand reduced the production of intestinal mucus and increased the risk of microbial invasion, which in turn affected the immune cell differentiation and cytokine production (61, 62). The cytokine IL-17A is a regulator of the fatty acid transporter *Cd36* and lipid absorption can be promoted by reducing the inhibition of *Cd36* expression by IL-17A (54). The decreased IL-17A level and increased *Cd36* expression in prediabetes mice indicated that the specific gut microbiota promoted the absorption of excess PA by disrupting the integrity of the intestinal mucous layer and regulating the expression of IL-17A and *Cd36*. In addition, the beneficial bacteria decreased in abundance in T2DM macaques and prediabetes mice. These beneficial bacteria, such as *F. succinogenes*, Christensenellaceae, and F16, protect the mucosal barrier and improved insulin resistance (63, 64, 65). We inferred the collectively effects of these gut microbes

401 determined the absorption of excess PA from ileum to serum, which might contribute
402 to the development of T2DM.

403 In conclusion, spontaneous T2DM macaques that have never been treated with
404 diabetes-related drugs provide a valuable model for our understanding of the
405 pathological characteristics and pathogenesis of T2DM. This study characterized
406 changes in gene expression, metabolites, and gut microbiota levels of spontaneous
407 T2DM macaques using multi-omics techniques. We found gut abnormal microbiota,
408 tryptophan metabolism and fatty acid β oxidation disorders, inflammation, and PA
409 accumulation. We also successfully induced prediabetes in mice by transplanting fecal
410 microbiota from T2DM macaques into antibiotic pretreated mice fed a high PA diet.
411 Our study confirms the causative effect of gut microbiota composition change and PA
412 in T2DM development. The microbiota composition, specifically higher abundance of
413 *R. gnavus* and *Coprococcus* sp. and lower abundance of *Treponema*, *F. succinogenes*,
414 Christensenellaceae and F16, promoted the absorption of excess PA thus led to the
415 development of T2DM. This study provides new insights into the interaction of gut
416 microbiota and metabolites in the development of T2DM, which expands our
417 understanding of the pathogenesis of this metabolic disease and may provide novel
418 insights for the treatment of T2DM in the future.

419 **Materials and methods**

420 **The screening of spontaneous T2DM macaques**

421 The experimental macaques used in this study were all from Greenhouse
422 Biotechnology Co., LTD (Meishan, China). We obtained eight spontaneous T2DM
423 macaques with FPG≥7 mmol/L and eight heathy control macaques with FPG≤6.1
424 mmol/L (three consecutive detections, each detection interval of one month) from a
425 population of 1698 captive macaques. None of these 16 screened macaques received
426 any medical treatment for diabetes.

427 **Sample collection**

428 Each experimental macaque was kept in a single cage, and was fasted for 12 hours but
429 had free access to drinking water. We obtained serum, plasma and whole blood for the

detection of physiological and biochemical parameters, and metabolome and transcriptome analysis. Fecal samples were collected within ten minutes after deposition. During the sampling process, fecal samples were loaded into a 50 mL sterile centrifuge tube were stored at -80℃. We followed animal welfare guidelines throughout the sample collection process, and all observations and samplings were approved by the Sichuan University's Animal Care Committee.

Physiological and biochemical parameters

In this study, FGP, HbA1c and FPI were detected by hexokinase method, high performance liquid chromatography and electro-chemiluminescence method, respectively. TC, TG, HDL and LDL were detected by automatic biochemical analyzer. HOMA-IR is one of the criteria for T2DM, calculated as: (FPI×FPG)/22.5.

Feces 16S rRNA amplicon sequencing and analysis

Total DNA from fecal samples was extracted using the QIAamp Fast DNA Stool Mini Kit. The V3-V4 region of the 16S rRNA gene was amplified using the 341F/806R primer (341F: 5'-CCTAYGGGRBGCASCAG -3', 806R: 5'-GGACTACNNGGGTATCTAAT -3'). The purification and quantification of the amplified products were performed and followed by the sequencing library preparation with TruSeq Nano DNA LT Library Prep Kit (Illumina, USA). The library sequencing was performed on Illumina MiSeq platform and 250 bp paired-end reads were generated. Raw sequencing reads were merged using FLASH (VI.2.7, http://ccb.jhu.edu/software/FLASH/) (66) and analyzed by QIIME2 (version 2020.11.1) pipeline with default parameters. Reads after denoising by DADA2 were clustered into OTUs at 99% similarity threshold. Taxonomy of OTUs was assigned based on Greengenes reference database (67). The QIIME2 diversity plugin was used to calculate alpha diversity (68). Principal Coordinate Analysis (PCoA) was determined by using the R package vegan. Differentially microbes were determined using linear discriminant analysis effect size (LEfSe) (69).

Feces shotgun metagenome sequencing and analysis

Total DNA from each sample was extracted using Tiangen DNA Stool Mini Kit

(Tiangen Biotech Co., Ltd., China). Metagenome sequencing was performed using the Illumina NovaSeq 6000 platform with a paired-end sequencing length of 150 bp. Trimmomatic was used for removing the adapters and low-quality raw reads based on a four-base wide sliding window, with average quality per base>20 and minimum length 90 bp (70). The rhesus macaque potential sequences were removed using Bowtie2 (71) with the reference genome (assembly Mmul_10). Taxonomy of remaining reads was assigned using Kraken2 (72) with the option "--use-mpa-style". *De novo* assembly of remaining reads was performed using MEGAHIT (73) with the option "-m 0.90 --min-contig-len 300". Prodigal (74) was used for gene prediction. The construction of non-redundant gene catalogue was performed with CD-HIT (75) with the option "-c 0.95 -aS 0.90". Quantification of the non-redundant genes in each sample was performed using Salmon (76). The amino acid sequences translated from non-redundant genes were aligned (--id 80% --query-cover 70% --evalue 1e-5) by DIAMOND (77) in the Carbohydrate-Active enZYmes (CAZy) database (78). The annotation metabolic pathway was performed using HUMANn3 (79).

RNA sequencing and DEG analysis

Total RNA was extracted using PAXgene Blood RNA kit. The cDNA Library was constructed following the NEBNext® UltraTM RNA Library Prep Kit for Illumina® (NEB, USA) manual, and index was added to each sample for sample differentiation. cBot Cluster Generation System was used to cluster the sequences with the same index. Illumina Hiseq 2500 sequencing platform was used to obtain the paired-end sequencing reads (PE150). NGS QC Toolkit v2.3.3 (80) was used to obtain high quality reads (high-quality paired reads with more than 90% of bases with Q-value≥20 were retained). Processed reads of each sample were mapped to the macaque reference genome using HISAT2 v2.1.0 (Kim, et al. 2015). Each alignment output file was assembled into a separate transcriptome using StringTie v1.3.6 (81), resulting in a transcript GTF file. To obtain the expression value of TPM (transcripts per million) and raw read counts of each gene, transcript GTF file was used as the reference annotation file. Differential expression analysis was performed using

DESeq2 R package (82). DEGs were screened according to Foldchange value (FC) and p value corrected by FDR (Benjamini-Hochberg method was selected) (adj $p<0.05$, $|\log2FC|>1$).

Weighted Gene Co-Expression Network Analysis (WGCNA) (83) was used to analyse the correlation between genes and phenotypes. We selected an appropriate "soft thresholding power" using the "picksoftthreshold" function in the WGCNA package (v1.61). Next, "blockwiseModules" function was used to construct the co-expression matrix with the option "checkMissingData=TRUE, power=16, TOMType='unsigned', minModuleSize=30, maxBlockSize=6000, mergeCutHeight=0.25". The modules with high correlation to T2DM phenotype and $p<0.05$ were selected for downstream analysis, and genes in these modules were used for GO and KEGG functional enrichment analysis. Hub genes were identified based on the module eigengene-based connectivity (kME), |kME>0.8| as the cut-off criteria.

Instead of identifying the differentially expressed genes within a pathway between the two groups, Aggregate Fold Change (AFC) calculated the average multiple change for each gene and defined the pathway score as the average difference multiple for all genes in that pathway. A null hypothesis test was performed using the pathway scores of the gene expression dataset, and the significance of each pathway was estimated by p-value (84). STRING (v11.0) provides a tool for functional enrichment analysis based on AFC. GO and KEGG enrichment analysis was performed using g: Profiler (85), AFC enrichment analysis was performed using STRING (https://www.string-db.org/cgi/input?sessionId=bfRWW6asD8S4&input_page_show_search=on).

Untargeted metabolomics processing

The 200 μL homogenized fecal sample was mixed with 800 μL cold methanol/acetonitrile (1:1, v/v) to remove the protein. The mixture was centrifuged for 15 min (14000g, 4°C) followed by the drying of the supernatant in a vacuum centrifuge. For LC-MS analysis, the samples were re-dissolved in 100 μL

acetonitrile/water (1:1, v/v) solvent. LC-MS/MS analysis was performed using an UHPLC (1290 Infinity LC, Agilent Technologies) coupled to a quadrupole time-of-flight (AB Sciex TripleTOF 6600) in Shanghai Applied Protein Technology Co., Ltd. The samples were separated by Agilent 1290 Infinity LC ultra-high performance liquid chromatography (UHPLC) HILIC column. In both ESI positive and negative modes, the mobile phase contained A=25 mM ammonium acetate and 25 mM ammonium hydroxide in water and B=acetonitrile. The gradient was 85% B for 1 min and was linearly reduced to 65% in 11 min, and then was reduced to 40% in 0.1 min and kept for 4 min, and then increased to 85% in 0.1 min, with a 5 min re-equilibration period employed. AB Triple TOF 6600 mass spectrometer was used to collect the primary and secondary spectra of per sample. After separation by UHPLC, the samples were analyzed by Triple TOF 6600 mass spectrometer (AB SCIEX). Positive and negative modes of electrospray ionization (ESI) were respectively detected.

Targeted medium-and long-chain fatty acid metabolomics processing

A total amount of 100 μL plasma per sample was taken in 2 mL glass centrifuge tubes and 1mL chloroform methanol solution was added. After 30min of ultrasound, the supernatant was taken and 2mL of 1% sulfuric acid-methanol solution was added. The mixed solution was placed in a water bath at 80℃, for 30min, and then 1mL of N-hexane and 5 mL of pure water were added in turn. Next, 500 μL of supernatant was absorbed, 25 μL of methyl N-nonaconate was added and mixed. The final sample was detected by GC-MS. All samples were separated by Agilent DB-WAX capillary column (30 m×0.25 mm ID×0.25 μm) gas chromatography. Agilent 7890/5975C gas-mass spectrometer was used for mass spectrometry. The chromatographic peak area and retention time were extracted by MSD ChemStation software. The content of medium-and long-chain fatty acids was calculated by drawing a standard curve.

Metabolomics statistical processing

The screening of significant changed metabolites was performed using univariate and multidimensional analysis. Student’s t test was applied to determine the significance

of differences between two groups. The variable importance in the projection (VIP) value of each variable was obtained from the Orthogonal Partial Least Squares Discriminant Analysis (OPLS-DA) model, which was used to indicate its contribution to the classification. The screening criteria were $p<0.05$ and VIP>1.

Animal treatments

Specific-pathogen-free C57BL/6J male mice at 6 weeks of age (vendor: Chengdu dossy experimental animals Co., LTD) were randomly assigned to four groups (FTPA, FT, PA and Control). All the mice lived in cages with the same conditions, including 12h light and 12h dark cycles, temperature 22-25 °C and humidity 40-60%.

Diets

HPAD was prepared by adding 12% PA to conventional forage. Both the conventional forage and the HPAD were sterile and the fresh forage was renewed three times a week. On day 0, the diets of FTPA-treated mice and PA-treated mice were switched to HPAD, FT-treated mice and control mice were still fed with conventional forage. Drinking water was sterile and renewed twice a day.

Transplant preparation and use

After single cage feeding, FPG detection and fecal collection were performed, and fecal samples of seven T2DM macaques were mixed for the preparation of transplants. The appropriate volume of diluent was added to the fecal sample (i.e. add 4 ml diluent per gram of feces) and the preparation of diluent can be found in (86). Sodium L-ascorbic acid and L-cysteine hydrochloride monohydrate were added to all suspensions at final concentrations of 5% (w/v) and 0.1% (w/v), respectively (The sterile diluent of control group was added with the same amount of reagent). The mixture was homogenized and filtered with a 200-mesh sterile mesh screen to remove large particles from the feces, and the filtrate was passed through 400 and 800 sterile mesh screens to remove undigested food and smaller particulate matter. The filtrate was divided into 50 ml centrifuge tubes, centrifuged at 600×g for 5 min, and the precipitation was discarded. Finally, the fecal supernatant was divided into new centrifuge tubes in equal parts (400 μL per tube) and frozen at -80°C. For use, the

transplant was quickly thawed in a 37℃ water bath.

Fecal microbiota transplantation (FMT)

After one week of changed feeding regime, the FTPA and FT mice groups were pre-treated with 1 g/L neomycin sulfate, 1 g/L ampicillin and 1 g/L metronidazole in the drinking water for 14 days, and the control group was not treated. For FMT treatment, the gavage with 400 μL transplant, which were thawed ahead of time, was performed for 14 days in FTPA and FT-treated mice. At the same time, the gavage in control and PA-treated mice were performed with sterile diluent.

Metabolic measurements

Throughout the experiment, body weight and feces were collected every month, FPG detection was every half month. OGTT was performed on day 110 and ITT was performed on day 115. For OGTT, after a 12h overnight fast, oral glucose gavage (1.2 g/kg of 12% dextrose solution) was performed and followed by blood sample collection from the tail vein at 0, 15, 30, 60, 90 and 120 min. For ITT, after a 6h fast, intraperitoneal insulin injection was performed (0.75 U/kg, human regular insulin), followed by the blood samples collection from the tail vein at 0, 20, 40, 60, 90 and 120 min. On day 120, after FPG detection, blood collection and issues were collected for quantitative RT-PCR, H-E staining and ELISA.

Isolation of tissue for quantitative RT-PCR and ELISA

Tissue was homogenized for RNA extraction, after adjusting the final concentration of RNA, and DNA reverse transcription was performed. Quantitative RT-PCR was performed on CFX Connect Real-Time PCR Detection System (Bio-rad, USA) using SYBR Green (Table 3-5). PA, IL-1β, IL-6, TNF-α and IL-17A were detected using Jiangsu Meimian ELISA kit and followed operator instructions.

H-E staining

The isolated livers and pancreas were dehydrated and embedded after fixation with formalin for 24 h. Paraffin-embedded livers and pancreas specimens were cut at a thickness of 3 μm. All sections were stained with hematoxylin then eosin, and finally microscopy and image acquisition were performed.

Statistical analysis

In this study, one-way ANOVA was used to determine statistical significance for comparisons of more than three groups, and for comparisons of two groups, two-tailed t-test was used. p values are represented on figures as follows: ns, not significant, $*p<0.05$, $**p<0.01$.

Data availability

The raw data of transcriptomes, metagenomes, and 16S rRNA have been submitted to the China National Center for Bioinformation/Beijing Institute of Genomics, Chinese Academy of Sciences with BioProject accession no. PRJCA021499. We provide four links that reviewers can use to access the raw data. Transcriptomes data: https://ngdc.cncb.ac.cn/gsa/s/4xAVJ3Lk (GSA: CRA013604). 16S rRNA data (macaque): https://ngdc.cncb.ac.cn/gsa/s/bsDz9qrN (GSA: CRA013637). 16S rRNA data (mouse): https://ngdc.cncb.ac.cn/gsa/s/1YcuC464 (GSA: CRA013638). metagenomes data: https://ngdc.cncb.ac.cn/gsa/s/3k38T849 (GSA: CRA013607). The identified untargeted metabolites were listed in the Table S4. The identified targeted medium-and long-chain fatty acid metabolites were listed in the Table S5.

Acknowledgements

This work was supported by the Science and Technology Foundation of Sichuan Province (2021YJ0136) and the National Natural Science Foundation of China (No. 32171607). Special thanks to Sichuan Green-house Biotech Co., Ltd. for the sample collection and thanks to Prof. Jinchuan Xing and Dr. Megan Price for revising the manuscript.

Author contributions

X.L., G.H., Q.H.L., S.Z.Y. and C.J. collected the samples; X.L. and S.Z.Y. performed the bioinformatics analyses; X.L., Y.C.X., K.S., C.J., J.X.L. and L.Z. performed the experiments; X.L. wrote the manuscript; J.L., Z.L.H., Z.X.F. and B.S.Y. revised the

632 manuscript; J.L. conceived and designed the experiments.

633 **Declaration of interests**

634 The authors declare no competing interests.

635 **Figure legends**

636 **Figure 1. The changes in gut microbiota in spontaneous T2DM macaques.**

637 (A) Alpha diversity estimates (Shannon index) between T2DM and control groups (ns,
638 not significant, two-tailed t-test, n=8).

639 (B) Alpha diversity estimates (Simpson index) between T2DM and control groups (ns,
640 not significant, two-tailed t-test, n=8).

641 (C) Principal Coordinate Analysis (PCoA) (n=8).

642 (D) Differential analysis of gut microbial composition in T2DM and control groups
643 (n=8).

644 (E) LEfSe analysis between T2DM and control groups (n=8).

645 (F) Differential analysis of gut microbial function in T2DM and control groups (n=5).
646 The pathways with red color were associated with T2DM and inflammation. Error bar
647 is mean with ± standard deviation (s.d.).

648 (G) Differential analysis of gut microbial CAZy enzyme in T2DM and control groups
649 (n=5). CBMs: carbohydrate-binding module (p=0.022, two-tailed t-test); GTs:
650 Glycosyl Transferases (p=0.013, two-tailed t-test); PLs: Polysaccharide Lyases
651 (p=0.017, two-tailed t-test); AA: Auxiliary activity enzymes (ns, not significant,
652 two-tailed t-test); GH: Glycoside hydrolases (ns, not significant, two-tailed t-test); CE:
653 Carbohydrate esterases (p=0.039, two-tailed t-test). For all boxplots: centre lines, upper
654 and lower bounds show median values, 25th and 75th quantiles; upper and lower
655 whiskers show the largest and smallest non-outlier values. In c, ellipses represent the
656 95% confidence intervals.

Figure 2. The alterations of fecal metabolites and gene expression in spontaneous T2DM macaques.

(A) Orthogonal partial least squares discriminant analysis (OPLS-DA) score plots based on the metabolic profiles.

(B) Volcano plots of metabolomics (p<0.05, two-tailed t-test).

(C) Fecal metabolites with significant differences between T2DM and control groups (VIP>1, p<0.05, two-tailed t-test).

(D) Enrichment analysis of the differentially abundant pathways between T2DM and control groups (p<0.05, two-tailed t-test).

(E) Non-metric multidimensional scaling (NMDS) analysis between T2DM and control groups (p=0.019, two-tailed t-test).

(F) Volcano plots of DEGs (log fold change≥1, p<0.05, two-tailed t-test).

(G) The GO and KEGG pathway enrichment analyses (p<0.05, two-tailed t-test).

(H) Weighted Gene Co-Expression Network Analysis (WGCNA).

(I) Venn analysis between hub genes and DEGs. In A and E, ellipses represent the 95% confidence intervals. Data shown are from 8 individuals per group.

Figure 3. LCFAs accumulation and inflammation occurred in spontaneous T2DM macaques.

(A-E) The contents of SFA (A, p=0.038), MUFA (B), PUFA (C), N3 (D), and N6 (E) in plasma (ns, not significant, two-tailed t-test).

(F) The univariate analysis by two-tailed t-test, error bar is mean with ± s.d.

(G) The multidimensional analysis by VIP value (VIP>1).

(H-J) The contents of serum inflammatory cytokines, including IL-1β (H, p=0.032), TNF-α (I) and IL-6 (J) (ns, not significant, two-tailed t-test).

(K) Correlation analysis between DEGs, differential metabolites, and differential microbes using Spearman rank correlation (|r|>0.5, adj p<0.05). For all boxplots: centre lines, upper and lower bounds show median values, 25th and 75th quantiles; upper and lower whiskers show the largest and smallest non-outlier values. Data shown are from 7 individuals per group.

Figure 4. The FMT and high PA diet mice developed pre-T2DM characteristics.

(A) Experimental scheme of FMT and high PA diet treatment.

(B-H) Metabolic analysis, including the trend of FPG within 120 days (B), FPG (C, p=0.0003), OGTT (D), AUC of OGTT (E, p=0.028), FPI (F, p=0.007), ITT (G), and body weight change (H) on day 120.

(I-J) The contents of TC (I, p=0.005) and TG (J, p=0.041) in serum on day 120.

(K and L) Representative H-E staining images of liver (K) and pancreas (L). For all boxplots: centre lines, upper and lower bounds show median values, 25th and 75th quantiles; upper and lower whiskers show the largest and smallest non-outlier values. Significance was determined using one-way ANOVA. In d, g, and h: *p<0.05, **p<0.01. Data shown are from 4-6 individuals per group.

Figure 5. The PA accumulation required the specific gut microbiota.

(A-C) Total PA contents in serum (A, p=0.013), ileum (B, p=0.016) and feces (C, p=0.014) on day 120.

(D) Quantitative RT-PCR for Cd36 transcripts in ileum on day 120 (p=0.049).

(E) The content of IL-17A in ileum on day 120 (p=0.027). For all boxplots: centre lines, upper and lower bounds show median values, 25th and 75th quantiles; upper and lower whiskers show the largest and smallest non-outlier values. Significance was determined using one-way ANOVA. Data shown are from 3-4 individual macaques per group.

(F) NMDS analysis (p=0.001, one-way ANOVA), ellipses represent the 95% confidence intervals.

(G and H) LEfSe analysis between FTPA and control groups (G), FT and control groups (H). Data shown are from 4 individuals per group.

(I) Specific gut microbiota structure promoted the absorption of excess PA by regulating the expression of IL-17A and *Cd36*, leading to the LCFAs accumulation and insulin resistance.

Figure 6. Integration of multi-omics results.

(A) Insulin resistance, fatty acid oxidation disorders, LCFAs accumulation and inflammation occurred in spontaneous T2DM macaques.

(B) Incomplete mitochondrial LCFAs β oxidation. The expression levels of fatty acid metabolism-related genes HADHB and ACSM3 were downregulated in spontaneous T2DM macaques, which could lead to accumulation of acylcarnitine, including l-propionylcarnitine, hexanoyl-l-carnitine, (r)-butyrylcarnitine, and isovaleryl-l-carnitine.

(C) Gut inflammation. The decrease of Lactobacillus sp. likely caused the reduction of serotonin and indole-3-acetaldehyde, which promotes the expansion of PA producer Erysipelotrichacea and ultimately led to PA accumulation. Both Erysipelotrichacea and Ruminococcus gnavus promote the development of inflammation. Accumulation of PA and inflammation are important factors in the development of T2DM.

(D) Accumulation of PA promoted the development of insulin resistance. In the PA-mTORC1-Akt pathway, the changes of RAP1A, SESTRIN3, and IRS1 expression promoted the development of insulin resistance in spontaneous T2DM macaques. The increase of PA promoted the development of T2DM by up-regulating the NF-κB signaling pathway.

Tables

Table 1 Physiological and biochemical parameters of Control and T2DM group

Index	T2DM (n=8)	Control (n=8)
FPG (mmol/L)	7.75±1	4.05±1.02**
FPI (μU/mL)	17.97±8.50	6.45±2.56**
HOMA-IR	6.24±3.06	1.20±0.65**
BMI	14.03±7.71	14.30±1.42
HbA1c (%)	3.78±0.70	3.26±0.62
TG (mmol/L)	0.97±0.53	0.68±0.42
TC (mmol/L)	3.30±0.98	3.52±0.86
HDL (mmol/L)	1.23±0.40	1.42±0.38
LDL (mmol/L)	1.36±0.44	1.47±0.57

735 * $p<0.05$, ** $p<0.01$

736 FPG: fasting plasma glucose; FPI: fasting plasma insulin; HOMA-IR:
737 homeostasismodel assessment- insulin resistance; BMI: body mass index; HbA1c:
738 glycosylated hemoglobin A1c; TG: triglycerides; TC: total cholesterol; HDL:
739 high-density lipoprotein cholesterol; LDL: low-density lipoprotein cholesterol.

740

741 **Table 2 blood routine examination of Control and T2DM group**

Index	T2DM (n=7)	Control (n=7)
WBC (10e9/L)	15.63±4.66	11.32±2.19*
RBC (10e12/L)	5.47±0.51	5.77±0.43
HGB (g/L)	129.57±15.48	136.71±9.60
HCT (%)	41.31±3.64	44.22±3.12
MCV (fl)	74.13±2.49	76.74±2.00
MCH (pg)	23.17±1.00	23.71±0.60
MCHC (g/L)	312.86±10.16	309±8.14

RDW (%)	15.23±2.12	14.69±1.74
PLT (10e9/L)	402±86.66	371.57±86.42
MPV (fl)	10.54±1.62	10.24±1.12
PCT (%)	0.42±0.08	0.38±0.09
PDW (%)	14.94±0.58	14.83±1.64
LYM% (%)	23.67±10.26	47.71±8.13**
LYM# (10e9/L)	3.46±1.66	5.39±1.52*
MON% (%)	4.18±3.34	6.18±2.29
MON# (10e9/L)	0.65±0.62	0.71±0.38
NEU% (%)	71.13±13.23	44.28±8.96**
NEU# (10e9/L)	11.36±4.91	5.00±1.38**
EOS% (%)	0.91±0.69	1.50±1.94
EOS# (10e9/L)	0.14±0.12	0.17±0.22
BAS% (%)	0.12±0.13	0.33±0.47
BAS# (10e9/L)	0.02±0.02	0.04±0.07
NRBC# (10e9/L)	0	0
NRBC% (%)	0	0

* $p<0.05$, ** $p<0.01$

WBC: white blood cell; RBC: red blood cell; HGB: hemoglobin; HCT: hematocrit; MCV: mean corpuscular volume; MCH: mean corpuscular hemoglobin; MCHC: mean corpuscular hemoglobin concentration; RDW: red blood cell distribution width; PLT: platelet; MPV: mean platelet volume; PCT: procalcitonin; PDW: platelet volume distribution width; LYM%: lymphocyte percentage; LYM#: lymphocyte value; MON%: monocytes percentage; MON#: monocytes value; NEU%: neutrophil percentage; NEU#: neutrophil value; EOS%: eoseosinophil percentage; EOS#: eoseosinophil value; BAS%: basophil percentage; BAS#: basophil value; NRBC%: nucleated red blood cell percentage; NRBC#: nucleated red blood cell value.

Table 3 Primers of RT-PCR

Gene name	Sequences of primers
CD36/F	5'-ATGGGCTGTGATCGGAACTG-3'
CD36/R	5'-GTCTTCCCAATAAGCATGTCTCC-3'
GADPH/F	5'-CCTCGTCCCGTAGACAAAATG-3'
GADPH/R	5'-TCTCCACTTTGCCACTGCAA-3'

754 **Table 4 RT-PCR reaction components**

Reagent	Volume
2×SG Fast qPCR Master Mix	10.0 μL
DNF Buffer	2.0 μL
F primer (10umol/L)	0.4 μL
R primer (10umol/L)	0.4 μL
cDNA	1.0 μL
ddH_2O	6.2 μL

755 **Table 5 RT-PCR cycle procotol**

Step	Temperature	Time
1	95℃	3 min
2	95℃	1-3 s
3	60℃	30 s
4		
5	72℃	1 min

756

757

758 **Supplementary Figures**

759 **Figure S1 Metagenome analysis of microbiota.**

760 (A) Differential microbes screened by metagenome analysis ($p<0.05$, two-tailed t-test).

761 T2DM: type 2 diabetes mellitus

762 (B) The proportion of all metabolites.

763 (C) Correlation analysis between differential untargeted metabolites and differential

764 microbes (Spearman's Rho).

765 (D) Correlation analysis between differential targeted metabolites and differential

766 microbes (Spearman's Rho), *p<0.05. Data shown are from 5 individuals per group.

767 **Figure S2 Pathway enrichment analysis by AFC and WGCNA.**

768 (A) Total 26 differential pathways were enriched (FDR<0.05).

769 (B) The changes of gene expression in insulin resistance pathway compared to the

770 control group, red color illustrating the up-regulation of genes and blue showed the

771 down-regulation of genes in T2DM group, and the darker the color of the genes, the

772 greater the $|\log_{10}FC|$ value.

773 (C)WGCNA functional enrichment. Data shown are from 8 individuals per group.

774 **Figure S3 The changes in gut microbiota in FTPA, FT, and PA-treated mice.**

775 (A) Alpha diversity estimates (Shannon index) (p>0.05, one-way ANOVA, n=4).

776 (B) Alpha diversity estimates (Simpson index) between T2DM and control groups

777 (p>0.05, one-way ANOVA, n=4).

778 (C) Family level taxonomy and relative abundance of five groups.

779 (D) The changes of members of Lachnospiraceae family from day -14 to day 120.

780 (E) LEfSe analysis between PA and control groups. Data shown are from 4

781 individuals per group.

782 **Supplementary Tables: Table. S1.xlsx- Table. S5.xlsx**

783 Table S1. Information on the macaque samples.

784 Table S2. List of 64 differential metabolites.

785 Table S3. List of genes in four modules significantly correlated with T2DM.

Table S4. List of all identified untargeted metabolites.

Table S5. List of all targeted medium-and long-chain fatty acid metabolites.

References

1.Rayburn, W.F. (1997). Diagnosis and classification of diabetes mellitus: highlights from the American Diabetes Association. J Reprod Med *42*, 585–586.

2.Zhang, L., Chu, J., Hao, W., Zhang, J., Li, H., Yang, C., Yang, J., Chen, X., and Wang, H. (2021). Gut microbiota and type 2 diabetes mellitus: Association, mechanism, and translational applications. Mediators Inflamm. *17*, e5110276. https://doi.org/10.1155/2021/5110276.

3.Kahn, S.E., Cooper, M.E., and Del Prato, S. (2014). Pathophysiology and treatment of type 2 diabetes: perspectives on the past, present, and future. Lancet *383*, 1068–1083. https://doi.org/10.1016/s0140-6736(13)62154-6.

4.Kang, N., Chen, G., Tu, R., Liao, W., Liu, X., Dong, X., Li, R., Pan, M., Yin, S., Hu, K., et al. (2022). Adverse associations of different obesity measures and the interactions with long-term exposure to air pollutants with prevalent type 2 diabetes mellitus: The Henan Rural Cohort study. Environ. Res. *207*, 112640. https://doi.org/10.1016/j.envres.2021.112640.

5.Qin, J., Li, Y., Cai, Z., Li, S., Zhu, J., Zhang, F., Liang, S., Zhang, W., Guan, Y., Shen, D., et al. (2012). A metagenome-wide association study of gut microbiota in type 2 diabetes. Nature *490*, 55–60. https://doi.org/10.1038/nature11450.

6.Zhao, L., Zhang, F., Ding, X., Wu, G., Lam, Y.Y., Wang, X., Fu, H., Xue, X., Lu, C., Ma, J., et al. (2018). Gut bacteria selectively promoted by dietary fibers alleviate type 2 diabetes. Science *359*, 1151–1156. https://doi.org/10.1126/science.aao5774.

7.Karlsson, F.H., Tremaroli, V., Nookaew, I., Bergström, G., Behre, C.J., Fagerberg, B., Nielsen, J., and Bäckhed, F. (2013). Gut metagenome in European women with normal, impaired and diabetic glucose control. Nature *498*, 99–103. https://doi.org/10.1038/nature12198.

814 8.Tilg, H., and Moschen, A.R. (2014). Microbiota and diabetes: an evolving
815 relationship. Gut *63*, 1513–1521. https://doi.org/10.1136/gutjnl-2014-306928.
816 9.Hendrikx, T., and Schnabl, B. (2019). Indoles: metabolites produced by intestinal
817 bacteria capable of controlling liver disease manifestation. J. Intern. Med. *286*, 32–40.
818 https://doi.org/10.1111/joim.12892.
819 10.Qi, Q., Li, J., Yu, B., Moon, J., Chai, J.C., Merino, J., Hu, J., Ruiz-Canela, M.,
820 Rebholz, C., Wang, Z., et al. (2022). Host and gut microbial tryptophan metabolism
821 and type 2 diabetes: an integrative analysis of host genetics, diet, gut microbiome and
822 circulating metabolites in cohort studies. Gut *71*, 1098–1105.
823 https://doi.org/10.1136/gutjnl-2021-324053.
824 11.Wu, Z., Zhang, B., Chen, F., Xia, R., Zhu, D., Chen, B., Lin, A., Zheng, C., Hou,
825 D., Li, X., et al. (2023). Fecal microbiota transplantation reverses insulin resistance in
826 type 2 diabetes: A randomized, controlled, prospective study. Frontiers in Cellular and
827 Infection Microbiology 12. https://doi.org/10.3389/fcimb.2022.1089991.
828 12.Ng, S.C., Xu, Z., Mak, J.W.Y., Yang, K., Liu, Q., Zuo, T., Tang, W., Lau, L., Lui,
829 R.N., Wong, S.H., et al. (2021). Microbiota engraftment after faecal microbiota
830 transplantation in obese subjects with type 2 diabetes: a 24-week, double-blind,
831 randomised controlled trial. Gut *71*, 716–723.
832 https://doi.org/10.1136/gutjnl-2020-323617.
833 13.Ding, D., Yong, H., Na, Y., Lu, W., Xu, Y., Ye, X., Wang, Y., Cai, T., Zheng, X.,
834 Chen, H., et al. (2022). Prospective study reveals host microbial determinants of
835 clinical response to fecal microbiota transplant therapy in type 2 diabetes patients.
836 Front. Cell. Infect. Microbiol. *12*, 820367.
837 https://doi.org/10.3389/fcimb.2022.820367.
838 14.Unger, R.H., and Zhou, Y. (2001). Lipotoxicity of beta-cells in obesity and in other
839 causes of fatty acid spillover. Diabetes *50*, S118–S121.
840 https://doi.org/10.2337/diabetes.50.2007.s118.
841 15.Poitout, V., and Robertson, R.P. (2008). Glucolipotoxicity: fuel excess and β-cell
842 dysfunction. Endocr. Rev. *29*, 351–366. https://doi.org/10.1210/er.2007-0023.

16.Palomer, X., Pizarro-Delgado, J., Barroso, E., and Vázquez-Carrera, M. (2018). Palmitic and oleic acid: the yin and yang of fatty acids in type 2 diabetes mellitus. Trends Endocrinol. Metab. *29*, 178–190. https://doi.org/10.1016/j.tem.2017.11.009.

17.Milanski, M., Degasperi, G., Coope, A., Morari, J., Denis, R., Cintra, D.E., Tsukumo, D.M.L., Anhe, G., Amaral, M.E., Takahashi, H.K., et al. (2009). Saturated fatty acids produce an inflammatory response predominantly through the activation of TLR4 signaling in hypothalamus: implications for the pathogenesis of obesity. J. Neurosci. *29*, 359–370. https://doi.org/10.1523/jneurosci.2760-08.2009.

18.Fiehn, O., Garvey, W.T., Newman, J.W., Lok, K.H., Hoppel, C.L., and Adams, S.H. (2010). Plasma metabolomic profiles reflective of glucose homeostasis in non-diabetic and type 2 diabetic obese African-American women. PLoS One *5*, e15234. https://doi.org/10.1371/journal.pone.0015234.

19.Li, X., Xu, Z., Lu, X., Yang, X., Yin, P., Kong, H., Yu, Y., and Xu, G. (2009). Comprehensive two-dimensional gas chromatography/time-of-flight mass spectrometry for metabonomics: Biomarker discovery for diabetes mellitus. Anal. Chim. Acta *633*, 257–262. https://doi.org/10.1016/j.aca.2008.11.058.

20.Chandra, K., Jain, V., Azhar, M., Khan, W., Alam, O., Ahmad, S., and Jain, S.K. (2020). Effect of augmented glycation in mobilization of plasma free fatty acids in type 2 diabetes mellitus. Diabetes Metab Syndr *14*, 1385–1389. https://doi.org/10.1016/j.dsx.2020.07.028.

21.Ertunc, M.E., and Hotamisligil, G.S. (2016). Lipid signaling and lipotoxicity in metaflammation: indications for metabolic disease pathogenesis and treatment. J. Lipid Res. *57*, 2099–2114. https://doi.org/10.1194/jlr.r066514.

22.Salvadó, L., Palomer, X., Barroso, E., and Vázquez-Carrera, M. (2015). Targeting endoplasmic reticulum stress in insulin resistance. Trends Endocrinol. Metab. *26*, 438–448. https://doi.org/10.1016/j.tem.2015.05.007.

23.Tumova, J., Andel, M., and Trnka, J. (2016). Excess of free fatty acids as a cause of metabolic dysfunction in skeletal muscle. Physiol Res *65*, 193–207. https://doi.org/10.33549/physiolres.932993.

872 24.Cani, P.D., Amar, J., Iglesias, M.A., Poggi, M., Knauf, C., Bastelica, D., Neyrinck,
873 A.M., Fava, F., Tuohy, K.M., Chabo, C., et al. (2007). Metabolic endotoxemia
874 initiates obesity and insulin resistance. Diabetes *56*, 1761–1772.
875 https://doi.org/10.2337/db06-1491.
876 25.Birdwell, L., Levesque, D., Machiah, D., and Gumber, S. (2022).
877 Clinicopathologic characteristics of pancreatic islet amyloidosis in the rhesus
878 macaque (Macaca mulatta) and sooty mangabey (Cercocebus atys). J. Med. Primatol.
879 *51*, 155–164. https://doi.org/10.1111/jmp.12579.
880 26.Westermark, P., Andersson, A., and Westermark, G.T. (2011). Islet amyloid
881 polypeptide, islet amyloid, and diabetes mellitus. Physiol. Rev. *91*, 795–826.
882 https://doi.org/10.1152/physrev.00042.2009.
883 27.Cefalu, W.T. (2006). Animal models of type 2 diabetes: clinical presentation and
884 pathophysiological relevance to the human condition. ILAR J *47*, 186–198.
885 https://doi.org/10.1093/ilar.47.3.186.
886 28.Ji, F., Jin, L., Zeng, X., Zhang, X., Zhang, Y., Sun, Y., Gao, L., He, H., Rao, J., Liu,
887 X., et al. (2012). Comparison of gene expression between naturally occurring and
888 diet-induced T2DM in cynomolgus monkeys. Dongwuxue Yanjiu *33*, 79–84. doi:
889 10.3724/SP.J.1141.2012.01079.
890 29.Tang, MT. (2020). Study on the Role of Glucose and Lipid in the Establishment of
891 Type 2 Diabetic Cynomolgus Monkey Model. M.S. Thesis, Dept. Veterinary Med.,
892 South China Agricultural Univ. *2020*.
893 30.Du, Y., Gu, X., Meng, H., Aa, N., Liu, S., Peng, C., Ge, Y., and Yang, Z. (2018).
894 Muscone improves cardiac function in mice after myocardial infarction by alleviating
895 cardiac macrophage-mediated chronic inflammation through inhibition of NF-κB and
896 NLRP3 inflammasome. Am. J. Transl. Res. *10*, 4235–4246.
897 31.Alexeev, E.E., Lanis, J.M., Kao, D.J., Campbell, E.L., Kelly, C.J., Battista, K.D.,
898 Gerich, M.E., Jenkins, B.R., Walk, S.T., Kominsky, D.J., et al. (2018).
899 Microbiota-derived indole metabolites promote human and murine intestinal

900 homeostasis through regulation of interleukin-10 receptor. Am. J. Pathol. *188*, 1183–
901 1194. https://doi.org/10.1016/j.ajpath.2018.01.011.
902 32.Manzella, C., Singhal, M., Alrefai, W.A., Saksena, S., Dudeja, P.K., and Gill, R.K.
903 (2018). Serotonin is an endogenous regulator of intestinal CYP1A1 via AhR. Sci. Rep.
904 *8*, 6103. https://doi.org/10.1038/s41598-018-24213-5.
905 33.Natividad, J.M., Agus, A., Planchais, J., Lamas, B., Jarry, A.C., Martin, R., Michel,
906 M., Chong-Nguyen, C., Roussel, R., Straube, M., et al. (2018). Impaired aryl
907 hydrocarbon receptor ligand production by the gut microbiota is a key factor in
908 metabolic syndrome. Cell Metab. *28*, 737-749.e4.
909 https://doi.org/10.1016/j.cmet.2018.07.001.
910 34.Rutkowsky, J.M., Knotts, T.A., Ono-Moore, K.D., McCoin, C.S., Huang, S.,
911 Schneider, D., Singh, S., Adams, S.H., and Hwang, D.H. (2014). Acylcarnitines
912 activate proinflammatory signaling pathways. Am. J. Physiol. Endocrinol. Metab. *306*,
913 E1378–E1387. https://doi.org/10.1152/ajpendo.00656.2013.
914 35.Tilg, H., and Moschen, A.R. (2008). Inflammatory mechanisms in the regulation of
915 insulin resistance. Mol. Med. *14*, 222–231. https://doi.org/10.2119/2007-00119.tilg.
916 36.Koves, T.R., Ussher, J.R., Noland, R.C., Slentz, D., Mosedale, M., Ilkayeva, O.,
917 Bain, J., Stevens, R., Dyck, J.R.B., Newgard, C.B., et al. (2008). Mitochondrial
918 overload and incomplete fatty acid oxidation contribute to skeletal muscle insulin
919 resistance. Cell Metab. *7*, 45–56. https://doi.org/10.1016/j.cmet.2007.10.013.
920 37.Lee, Y., Kang, E.S., Kim, S.H., Han, S.J., Kim, C.H., Kim, H.J., Ahn, C.W., Cha,
921 B.S., Nam, M., Nam, C.M., et al. (2008). Association between polymorphisms in
922 SLC30A8, HHEX, CDKN2A/B, IGF2BP2, FTO, WFS1, CDKAL1, KCNQ1 and type
923 2 diabetes in the Korean population. J. Hum. Genet. *53*, 991–998.
924 https://doi.org/10.1007/s10038-008-0341-8.
925 38.Su, S., Zhang, C., Zhang, F., Li, H., Yang, X., and Tang, X. (2016). The association
926 between leptin receptor gene polymorphisms and type 2 diabetes mellitus: A
927 systematic review and meta-analysis. Diabetes Res. Clin. Pract. *121*, 49–58.
928 https://doi.org/10.1016/j.diabres.2016.08.008.

929 39.Zhao, J. (2014). Molecular mechanisms of AGE/RAGE-mediated fibrosis in the
930 diabetic heart. World J Diabetes *5*, 860. https://doi.org/10.4239/wjd.v5.i6.860.
931 40.Nascimento, E.B., Osler, M.E., and Zierath, J.R. (2013). Sestrin 3 regulation in
932 type 2 diabetic patients and its influence on metabolism and differentiation in skeletal
933 muscle. Am. J. Physiol. Endocrinol. Metab. *305*, E1408–E1414.
934 https://doi.org/10.1152/ajpendo.00212.2013.
935 41.Tabassum, R., Mahajan, A., Dwivedi, O.P., Chauhan, G., Spurgeon, C.J., Kumar,
936 M.V.K., Ghosh, S., Madhu, S.V., Mathur, S.K., Chandak, G.R., et al. (2012). Common
937 variants of SLAMF1 and ITLN1 on 1q21 are associated with type 2 diabetes in Indian
938 population. Am. J. Hum. Genet. *57*, 184–190. https://doi.org/10.1038/jhg.2011.150.
939 42.Junková, K., Mirchi, L.F., Chylíková, B., Janků, M., Šilhavý, J., Hüttl, M.,
940 Marková, I., Miklánková, D., Včelák, J., Malínská, H., et al. (2021). Hepatic
941 transcriptome profiling reveals lack of Acsm3 expression in polydactylous rats with
942 high-fat diet-induced hypertriglyceridemia and visceral fat accumulation. Nutrients *13*,
943 1462–1462. https://doi.org/10.3390/nu13051462.
944 43.Sekine, Y., Yamamoto, K., Kurata, M., Honda, A., Onishi, I., Kinowaki, Y.,
945 Kawade, G., Watabe, S., Nomura, S., Fukuda, S., et al. (2022). HADHB, a fatty acid
946 beta-oxidation enzyme, is a potential prognostic predictor in malignant lymphoma.
947 Pathology *54*, 286–293. https://doi.org/10.1016/j.pathol.2021.06.119.
948 44. Howson, J.M.M., Walker, N.M., Smyth, D.J., and Todd, J.A. (2009). Analysis of
949 19 genes for association with type I diabetes in the Type I Diabetes Genetics
950 Consortium families. Genes & Immunity *10*, S74–S84.
951 https://doi.org/10.1038/gene.2009.96.
952 45.Xu, L., Yin, L., Jin, Y., Qi, Y., Han, X., Xu, Y., Liu, K.X., Zhao, Y., and Peng, J.
953 (2020). Effect and possible mechanisms of dioscin on ameliorating metabolic
954 glycolipid metabolic disorder in type-2-diabetes. Phytomedicine *67*, 153139.
955 https://doi.org/10.1016/j.phymed.2019.153139.
956 46.Liu, L., Li, Y., Guan, C., Li, K., Wang, C., Feng, R., and Sun, C. (2010). Free fatty
957 acid metabolic profile and biomarkers of isolated post-challenge diabetes and type 2

958 diabetes mellitus based on GC–MS and multivariate statistical analysis. J. Chromatogr.
959 B *878*, 2817–2825. https://doi.org/10.1016/j.jchromb.2010.08.035.
960 47.Dinarello, C.A., Donath, M.Y., and Mandrup-Poulsen, T. (2010). Role of IL-1β in
961 type 2 diabetes. Curr Opin Endocrinol Diabetes Obes *17*, 1.
962 https://doi.org/10.1097/med.0b013e32833bf6dc.
963 48.Sun, J., Su, Y., Chen, J., Qin, D., Xu, Y., Chu, H., Lu, T., Dong, J., Qin, L., and Li,
964 W. (2023). Differential roles of CD36 in regulating muscle insulin response depend on
965 palmitic acid load. Biomedicines *11*, 729.
966 https://doi.org/10.3390/biomedicines11030729.
967 49.Kawano, Y., Edwards, M., Huang, Y., Bilate, A.M., Araujo, L.P., Tanoue, T.,
968 Atarashi, K., Ladinsky, M.S., Reiner, S.L., Wang, H.H., et al. (2022). Microbiota
969 imbalance induced by dietary sugar disrupts immune-mediated protection from
970 metabolic syndrome. Cell *185*, 3501-3519.e20.
971 https://doi.org/10.1016/j.cell.2022.08.005.
972 50.Hezaveh, K., Shinde, R.S., Klötgen, A., Halaby, M.J., Lamorte, S., Ciudad, M.T.,
973 Quevedo, R., Neufeld, L., Liu, Z.Q., Jin, R., et al. (2022). Tryptophan-derived
974 microbial metabolites activate the aryl hydrocarbon receptor in tumor-associated
975 macrophages to suppress anti-tumor immunity. Immunity *55*, 324-340.e8.
976 https://doi.org/10.1016/j.immuni.2022.01.006.
977 51.Brawner, K.M., Yeramilli, V.A., Duck, L.W., Van Der Pol, W., Smythies, L.E.,
978 Morrow, C.D., Elson, C.O., and Martin, C.A. (2019). Depletion of dietary aryl
979 hydrocarbon receptor ligands alters microbiota composition and function. Sci. Rep. *9*,
980 14724. https://doi.org/10.1038/s41598-019-51194-w.
981 52.Turpin, W., Bedrani, L., Espin-Garcia, O., Xu, W., Silverberg, M.S., Smith, M.I.,
982 Garay, J.A.R., Lee, S.H., Guttman, D.S., Griffiths, A., et al. (2020). Associations of
983 NOD2 polymorphisms with Erysipelotrichaceae in stool of in healthy first degree
984 relatives of Crohn's disease subjects. BMC Medical Genet. *21*, 204.
985 https://doi.org/10.1186/s12881-020-01115-w.

986 53.Turnbaugh, P.J., Bäckhed, F., Fulton, L., and Gordon, J.I. (2008). Diet-induced
987 obesity is linked to marked but reversible alterations in the mouse distal gut
988 microbiome. Cell Host Microbe *3*, 213–223.
989 https://doi.org/10.1016/j.chom.2008.02.015.
990 54.Zhang, H., DiBaise, J.K., Zuccolo, A., Kudrna, D., Braidotti, M., Yu, Y.,
991 Parameswaran, P., Crowell, M.D., Wing, R., Rittmann, B.E., et al. (2009). Human gut
992 microbiota in obesity and after gastric bypass. Proc. Natl. Acad. Sci. U.S.A. *106*,
993 2365–2370. https://doi.org/10.1073/pnas.0812600106.
994 55.López-Almela, I., Romaní-Pérez, M., Bullich-Vilarrubias, C., Benítez-PáezA.,
995 Gómez, E.M., Francés, R., Liebisch, G., and Sanz, Y. (2021). Bacteroides uniformis
996 combined with fiber amplifies metabolic and immune benefits in obese mice. Gut
997 Microbes *13*, 1–20. https://doi.org/10.1080/19490976.2020.1865706.
998 56.Kootte, R.S., Levin, E., Salojärvi, J., Smits, L.P., Hartstra, A.V., Udayappan, S.D.,
999 Hermes, G., Bouter, K.E., Koopen, A.M., Holst, J.J., et al. (2017). Improvement of
1000 insulin sensitivity after lean donor feces in metabolic syndrome is driven by baseline
1001 intestinal microbiota composition. Cell Metab. *26*, 611-619.e6.
1002 https://doi.org/10.1016/j.cmet.2017.09.008.
1003 57.Zhai, L., Xiao, H., Lin, C., Wong, H.L.X., Lam, Y.Y., Gong, M., Wu, G., Ning, Z.,
1004 Huang, C., Zhang, Y., et al. (2023). Gut microbiota-derived tryptamine and
1005 phenethylamine impair insulin sensitivity in metabolic syndrome and irritable bowel
1006 syndrome. Nat. Commun. *14*, 4986. https://doi.org/10.1038/s41467-023-40552-y.
1007 58.Paone, P., and Cani, P.D. (2020). Mucus barrier, mucins and gut microbiota: the
1008 expected slimy partners? Gut *69*, 2232–2243.
1009 https://doi.org/10.1136/gutjnl-2020-322260.
1010 59.Png, C.W., Lindén, S.K., Gilshenan, K.S., Zoetendal, E.G., McSweeney, C.S., Sly,
1011 L.I., McGuckin, M.A., and Florin, T.H.J. (2010). Mucolytic bacteria with increased
1012 prevalence in IBD mucosa augment in vitro utilization of mucin by other bacteria. Am.
1013 J. Gastroenterol. *105*, 2420–2428. https://doi.org/10.1038/ajg.2010.281.

1014 60.Henke, M.T., Kenny, D.J., Cassilly, C.D., Vlamakis, H., Xavier, R.J., and Clardy, J.
1015 (2019). Ruminococcus gnavus, a member of the human gut microbiome associated
1016 with Crohn's disease, produces an inflammatory polysaccharide. Proc. Natl. Acad. Sci.
1017 U.S.A. *116*, 12672–12677. https://doi.org/10.1073/pnas.1904099116.
1018 61.Yin, J., Yang, K., Zhou, C., Xu, P., Xiao, W., and Yang, H. (2019). Aryl
1019 hydrocarbon receptor activation alleviates dextran sodium sulfate-induced colitis
1020 through enhancing the differentiation of goblet cells. Biochem. Biophys. Res.
1021 Commun. *514*, 180–186. https://doi.org/10.1016/j.bbrc.2019.04.136.
1022 62.Ma, N., Guo, P., Zhang, J., He, T., Kim, S.W., Zhang, G., and Ma, X. (2018).
1023 Nutrients mediate intestinal bacteria–mucosal immune crosstalk. Front. Immunol. *9*, 5.
1024 https://doi.org/10.3389/fimmu.2018.00005.
1025 63.Oki, K., Toyama, M., Banno, T., Chonan, O., Benno, Y., and Watanabe, K. (2016).
1026 Comprehensive analysis of the fecal microbiota of healthy Japanese adults reveals a
1027 new bacterial lineage associated with a phenotype characterized by a high frequency
1028 of bowel movements and a lean body type. BMC Microbiol *16*, 284.
1029 https://doi.org/10.1186/s12866-016-0898-x.
1030 64.Miguel, M.A., Lee, S.S., Mamuad, L.L., Choi, Y.J., Jeong, C.D., Son, A., Cho,
1031 K.K., Kim, E.T., Kim, S.B., and Lee, S.S. (2019). Enhancing butyrate production,
1032 ruminal fermentation and microbial population through supplementation with
1033 Clostridium saccharobutylicum. J. Microbiol. Biotechnol. *29*, 1083–1095.
1034 https://doi.org/10.4014/jmb.1905.05016.
1035 65.Zhong, H., Wang, J., Abdullah, Hafeez, M.A., Guan, R., and Feng, F. (2021).
1036 Lactobacillus plantarum ZJUFB2 Prevents High Fat Diet-Induced Insulin Resistance
1037 in Association With Modulation of the Gut Microbiota. Front. Nutr. *8*, 75422.
1038 https://doi.org/10.3389/fnut.2021.754222.
1039 66.Magoc, T., and Salzberg, S.L. (2011). FLASH: fast length adjustment of short
1040 reads to improve genome assemblies. Bioinformatics *27*, 2957–2963.
1041 https://doi.org/10.1093/bioinformatics/btr507.

1042 67.McDonald, D., Price, M.N., Goodrich, J., Nawrocki, E.P., DeSantis, T.Z., Probst,
1043 A., Andersen, G.L., Knight, R., and Hugenholtz, P. (2011). An improved Greengenes
1044 taxonomy with explicit ranks for ecological and evolutionary analyses of bacteria and
1045 archaea. ISME J *6*, 610–618. https://doi.org/10.1038/ismej.2011.139.
1046 68.Bolyen, E., Rideout, J.R., Dillon, M.R., Bokulich, N.A., Abnet, C.C., Al-Ghalith,
1047 G.A., Alexander, H., Alm, E.J., Arumugam, M., Asnicar, F., et al. (2019).
1048 Reproducible, interactive, scalable and extensible microbiome data science using
1049 QIIME 2. Nat. Biotechnol. *37*, 852–857. https://doi.org/10.1038/s41587-019-0209-9.
1050 69.Segata, N., Izard, J., Waldron, L., Gevers, D., Miropolsky, L., Garrett, W.S., and
1051 Huttenhower, C. (2011). Metagenomic biomarker discovery and explanation. Genome
1052 Biol *12*, R60. https://doi.org/10.1186/gb-2011-12-6-r60.
1053 70.Bolger, A.M., Lohse, M., and Usadel, B. (2014). Trimmomatic: a flexible trimmer
1054 for Illumina sequence data. Bioinformatics *30*, 2114–2120.
1055 https://doi.org/10.1093/bioinformatics/btu170.
1056 71.Langmead, B., and Salzberg, S.L. (2012). Fast gapped-read alignment with Bowtie
1057 2. Nat. Methods *9*, 357–359. https://doi.org/10.1038/nmeth.1923.
1058 72.Wood, D.E., and Salzberg, S.L. (2014). Kraken: ultrafast metagenomic sequence
1059 classification using exact alignments. Genome Biol. *15*, R46.
1060 https://doi.org/10.1186/gb-2014-15-3-r46.
1061 73.Li, D., Liu, C.M., Luo, R., Sadakane, K., and Lam, T.W. (2015). MEGAHIT: an
1062 ultra-fast single-node solution for large and complex metagenomics assembly via
1063 succinct de Bruijn graph. Bioinformatics *31*, 1674–1676.
1064 https://doi.org/10.1093/bioinformatics/btv033.
1065 74.82.Hyatt, D., Chen, G.L., LoCascio, P.F., Land, M.L., Larimer, F.W., and Hauser,
1066 L.J. (2010). Prodigal: prokaryotic gene recognition and translation initiation site
1067 identification. BMC Bioinform. *11*, 119. https://doi.org/10.1186/1471-2105-11-119.
1068 75.Fu, L., Niu, B., Zhu, Z., Wu, S., and Li, W. (2012). CD-HIT: accelerated for
1069 clustering the next-generation sequencing data. Bioinformatics *28*, 3150–3152.
1070 https://doi.org/10.1093/bioinformatics/bts565.

76.Patro, R., Duggal, G., Love, M.I., Irizarry, R.A., and Kingsford, C. (2017). Salmon provides fast and bias-aware quantification of transcript expression. Nat. Methods *14*, 417–419. https://doi.org/10.1038/nmeth.4197.

77.Buchfink, B., Xie, C., and Huson, D.H. (2014). Fast and sensitive protein alignment using DIAMOND. Nat. Methods *12*, 59–60. https://doi.org/10.1038/nmeth.3176.

78.Lombard, V., Golaconda Ramulu, H., Drula, E., Coutinho, P.M., and Henrissat, B. (2013). The carbohydrate-active enzymes database (CAZy) in 2013. Nucleic Acids Res. *42*, D490–D495. https://doi.org/10.1093/nar/gkt1178.

79.Franzosa, E.A., McIver, L.J., Rahnavard, G., Thompson, L.R., Schirmer, M., Weingart, G., Lipson, K.S., Knight, R., Caporaso, J.G., Segata, N., et al. (2018). Species-level functional profiling of metagenomes and metatranscriptomes. Nat. Methods *15*, 962–968. https://doi.org/10.1038/s41592-018-0176-y.

80.Patel, R.K., and Jain, M. (2012). NGS QC Toolkit: a toolkit for quality control of next generation sequencing data. PLoS One *7*, e30619. https://doi.org/10.1371/journal.pone.0030619.

81.Pertea, M., Pertea, G.M., Antonescu, C.M., Chang, T.C., Mendell, J.T., and Salzberg, S.L. (2015). StringTie enables improved reconstruction of a transcriptome from RNA-seq reads. Nat. Biotechnol. *33*, 290–295. https://doi.org/10.1038/nbt.3122.

82.Love, M.I., Huber, W., and Anders, S. (2014). Moderated estimation of fold change and dispersion for RNA-seq data with DESeq2. Genome Biol. *15*. https://doi.org/10.1186/s13059-014-0550-8.

83.Langfelder, P., and Horvath, S. (2008). WGCNA: an R package for weighted correlation network analysis. BMC Bioinform *9*, 559. https://doi.org/10.1186/1471-2105-9-559.

84.Yu, C., Woo, H.J., Yu, X., Oyama, T., Wallqvist, A., and Reifman, J. (2017). A strategy for evaluating pathway analysis methods. BMC Bioinform *18*. https://doi.org/10.1186/s12859-017-1866-7.

85.Raudvere, U., Kolberg, L., Kuzmin, I., Arak, T., Adler, P., Peterson, H., and Vilo, J. (2019). g:Profiler: a web server for functional enrichment analysis and conversions of gene lists (2019 update). Nucleic Acids Res. *47*, W191–W198. https://doi.org/10.1093/nar/gkz369.

86.Berland, M., Cadiou, J., Levenez, F., Galleron, N., Quinquis, B., Thirion, F., Gauthier, F., Le Chatelier, E., Plaza Oñate, F., Schwintner, C., et al. (2021). High engraftment capacity of frozen ready-to-use human fecal microbiota transplants assessed in germ-free mice. Sci. Rep *11*, 4365. https://doi.org/10.1038/s41598-021-83638-7.

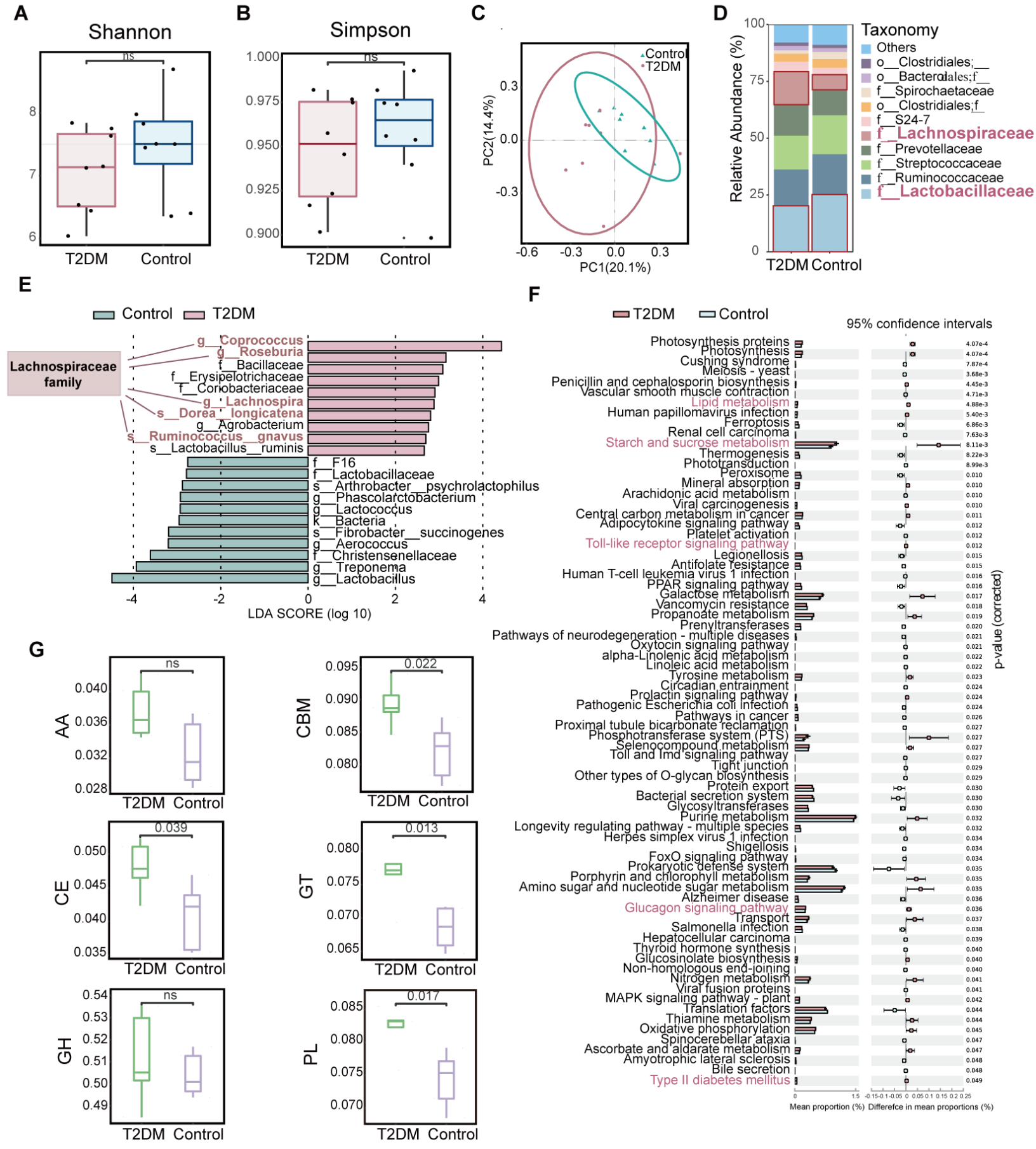
A
Shannon
ns
T2DM
Control
B
Simpson
ns
T2DM
Control
C
Control
T2DM
PC1(20.1%)
PC2(14.4%)
D
Taxonomy
Others
f__Spirochaetaceae
f__S24-7
f__Lachnospiraceae
f__Prevotellaceae
f__Streptococcaceae
f__Ruminococcaceae
f__Lactobacillaceae
Relative Abundance (%)
T2DM Control
E
Control
T2DM
Lachnospiraceae family
g__Coprococcus
g__Roseburia
f__Bacillaceae
f__Erysipelotrichaceae
f__Coriobacteriaceae
g__Lachnospira
s__Dorea_longicatena
g__Agrobacterium
s__Ruminococcus_gnavus
s__Lactobacillus_ruminis
f__F16
f__Lactobacillaceae
s__Arthrobacter_psychrolactophilus
g__Phascolarctobacterium
g__Lactococcus
k__Bacteria
s__Fibrobacter_succinogenes
g__Aerococcus
f__Christensenellaceae
g__Treponema
g__Lactobacillus
LDA SCORE (log 10)
F
T2DM
Control
95% confidence intervals
Photosynthesis proteins
Photosynthesis
Cushing syndrome
Meiosis - yeast
Penicillin and cephalosporin biosynthesis
Vascular smooth muscle contraction
Lipid metabolism
Human papillomavirus infection
Ferroptosis
Renal cell carcinoma
Starch and sucrose metabolism
Thermogenesis
Phototransduction
Peroxisome
Mineral absorption
Arachidonic acid metabolism
Viral carcinogenesis
Central carbon metabolism in cancer
Adipocytokine signaling pathway
Platelet activation
Toll-like receptor signaling pathway
Legionellosis
Antifolate resistance
Human T-cell leukemia virus 1 infection
PPAR signaling pathway
Galactose metabolism
Vancomycin resistance
Propanoate metabolism
Prenyltransferases
Pathways of neurodegeneration - multiple diseases
Oxytocin signaling pathway
alpha-Linolenic acid metabolism
Linoleic acid metabolism
Tyrosine metabolism
Circadian entrainment
Prolactin signaling pathway
Pathogenic Escherichia coli infection
Pathways in cancer
Proximal tubule bicarbonate reclamation
Phosphotransferase system (PTS)
Selenocompound metabolism
Toll and Imd signaling pathway
Tight junction
Other types of O-glycan biosynthesis
Protein export
Bacterial secretion system
Glycosyltransferases
Purine metabolism
Longevity regulating pathway - multiple species
Herpes simplex virus 1 infection
Shigellosis
FoxO signaling pathway
Prokaryotic defense system
Porphyrin and chlorophyll metabolism
Amino sugar and nucleotide sugar metabolism
Alzheimer disease
Glucagon signaling pathway
Transport
Salmonella infection
Hepatocellular carcinoma
Thyroid hormone synthesis
Glucosinolate biosynthesis
Non-homologous end-joining
Nitrogen metabolism
Viral fusion proteins
MAPK signaling pathway - plant
Translation factors
Thiamine metabolism
Oxidative phosphorylation
Spinocerebellar ataxia
Ascorbate and aldarate metabolism
Amyotrophic lateral sclerosis
Bile secretion
Type II diabetes mellitus
p-value (corrected)
Mean proportion (%)
Differefce in mean proportions (%)
G
AA
ns
CBM
0.022
CE
0.039
GT
0.013
GH
ns
PL
0.017
T2DM Control

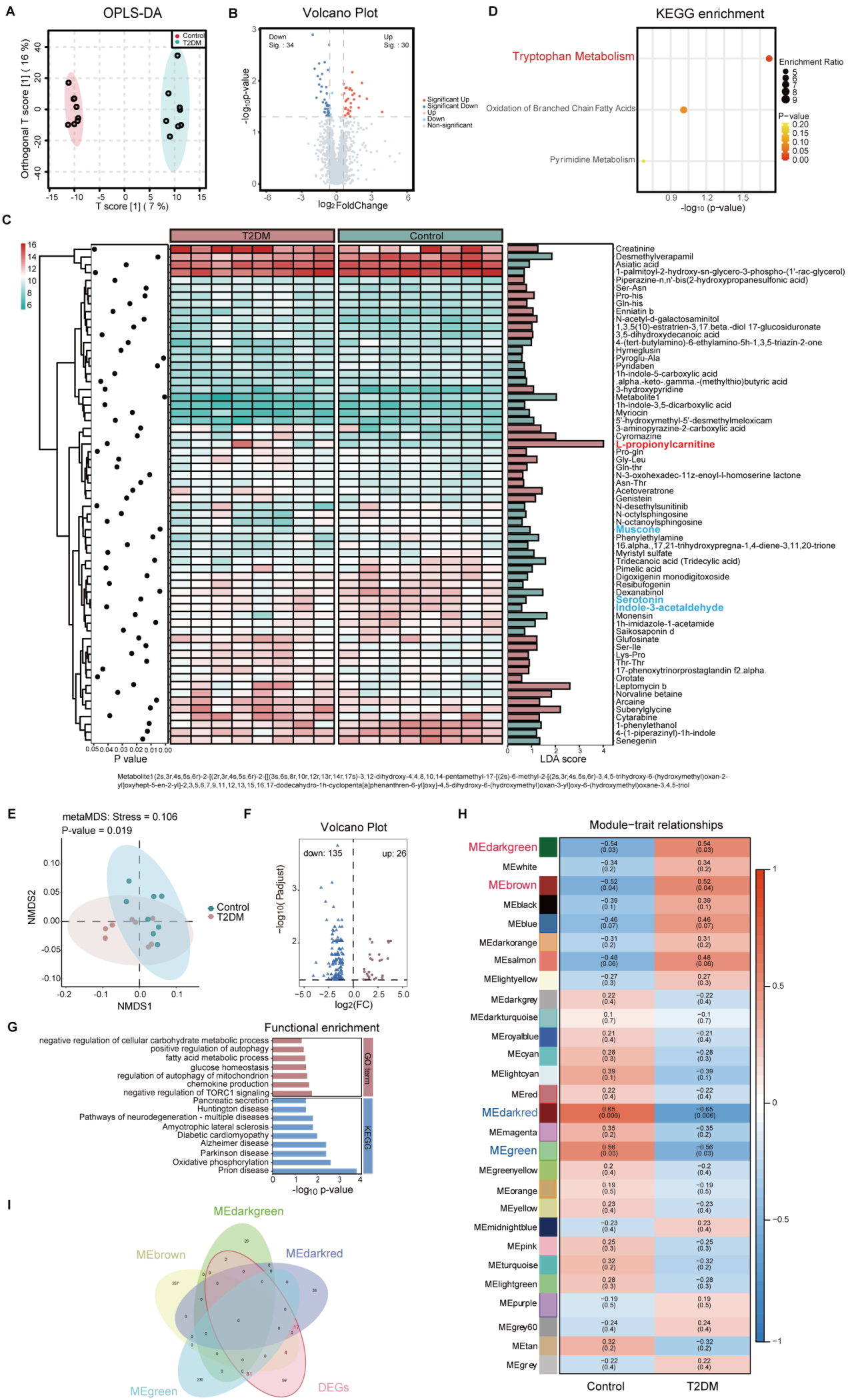
A
OPLS-DA
Control
T2DM
Orthogonal T score [1] (16 %)
T score [1] (7 %)
B
Volcano Plot
Down
Sig. : 34
Up
Sig. : 30
-log10P-value
log2FoldChange
Significant Up
Significant Down
Up
Down
Non-significant
D
KEGG enrichment
Tryptophan Metabolism
Oxidation of Branched Chain Fatty Acids
Pyrimidine Metabolism
Enrichment Ratio
P-value
-log10 (p-value)
C
T2DM
Control
P value
LDA score
Creatinine
Desmethylverapamil
Asiatic acid
1-palmitoyl-2-hydroxy-sn-glycero-3-phospho-(1'-rac-glycerol)
Piperazine-n,n'-bis(2-hydroxypropanesulfonic acid)
Ser-Asn
Pro-his
Gln-his
Enniatin b
N-acetyl-d-galactosaminitol
1,3,5(10)-estratrien-3,17.beta.-diol 17-glucosiduronate
3,5-dihydroxydecanoic acid
4-(tert-butylamino)-6-ethylamino-5h-1,3,5-triazin-2-one
Hymeglusin
Pyroglu-Ala
Pyridaben
1h-indole-5-carboxylic acid
.alpha.-keto-.gamma.-(methylthio)butyric acid
3-hydroxypyridine
Metabolite1
1h-indole-3,5-dicarboxylic acid
Myriocin
5'-hydroxymethyl-5'-desmethylmeloxicam
3-aminopyrazine-2-carboxylic acid
Cyromazine
L-propionylcarnitine
Pro-gln
Gly-Leu
Gln-thr
N-3-oxohexadec-11z-enoyl-l-homoserine lactone
Asn-Thr
Acetoveratrone
Genistein
N-desethylsunitinib
N-octylsphingosine
N-octanoylsphingosine
Muscone
Phenylethylamine
16.alpha.,17,21-trihydroxypregna-1,4-diene-3,11,20-trione
Myristyl sulfate
Tridecanoic acid (Tridecylic acid)
Pimelic acid
Digoxigenin monodigitoxoside
Resibufogenin
Dexanabinol
Serotonin
Indole-3-acetaldehyde
Monensin
1h-imidazole-1-acetamide
Saikosaponin d
Glufosinate
Ser-Ile
Lys-Pro
Thr-Thr
17-phenoxytrinorprostaglandin f2.alpha.
Orotate
Leptomycin b
Norvaline betaine
Arcaine
Suberylglycine
Cytarabine
1-phenylethanol
4-(1-piperazinyl)-1h-indole
Senegenin
Metabolite1 (2s,3r,4s,5s,6r)-2-[(2r,3r,4s,5s,6r)-2-[[(3s,6s,8r,10r,12r,13r,14r,17s)-3,12-dihydroxy-4,4,8,10,14-pentamethyl-17-[(2s)-6-methyl-2-[(2s,3r,4s,5s,6r)-3,4,5-trihydroxy-6-(hydroxymethyl)oxan-2-yl]oxyhept-5-en-2-yl]-2,3,5,6,7,9,11,12,13,15,16,17-dodecahydro-1h-cyclopenta[a]phenanthren-6-yl]oxy]-4,5-dihydroxy-6-(hydroxymethyl)oxan-3-yl]oxy-6-(hydroxymethyl)oxane-3,4,5-triol
E
metaMDS: Stress = 0.106
P-value = 0.019
NMDS2
NMDS1
Control
T2DM
F
Volcano Plot
down: 135
up: 26
-log10(Padjust)
log2(FC)
G
Functional enrichment
negative regulation of cellular carbohydrate metabolic process
positive regulation of autophagy
fatty acid metabolic process
glucose homeostasis
regulation of autophagy of mitochondrion
chemokine production
negative regulation of TORC1 signaling
Pancreatic secretion
Huntington disease
Pathways of neurodegeneration - multiple diseases
Amyotrophic lateral sclerosis
Diabetic cardiomyopathy
Alzheimer disease
Parkinson disease
Oxidative phosphorylation
Prion disease
GO term
KEGG
-log10 p-value
H
Module−trait relationships
MEdarkgreen
MEwhite
MEbrown
MEblack
MEblue
MEdarkorange
MEsalmon
MElightyellow
MEdarkgrey
MEdarkturquoise
MEroyalblue
MEcyan
MElightcyan
MEred
MEdarkred
MEmagenta
MEgreen
MEgreenyellow
MEorange
MEyellow
MEmidnightblue
MEpink
MEturquoise
MElightgreen
MEpurple
MEgrey60
MEtan
MEgrey
Control
T2DM
I
MEdarkgreen
MEbrown
MEdarkred
MEgreen
DEGs

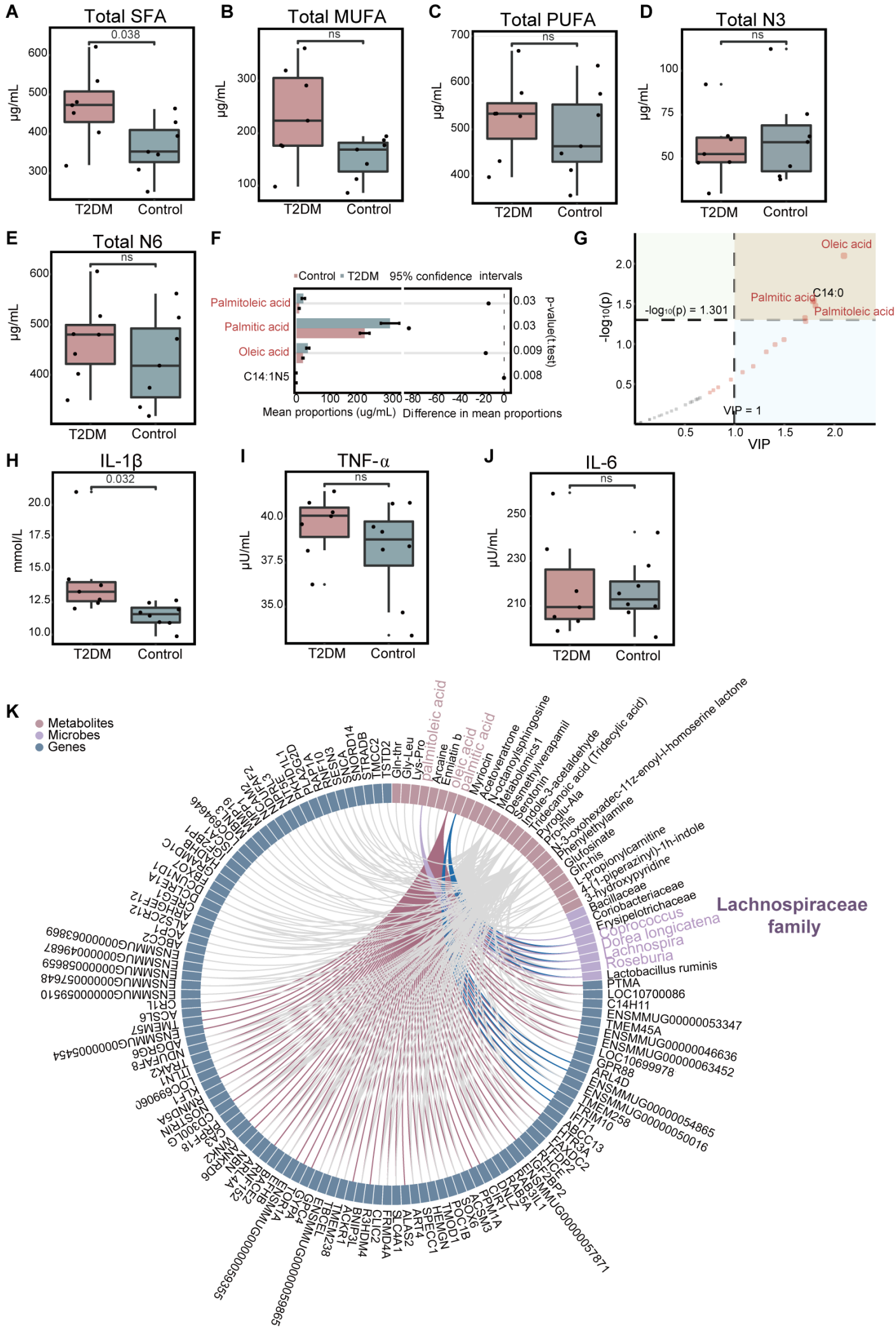
A
Total SFA
0.038
μg/mL
T2DM
Control
B
Total MUFA
ns
C
Total PUFA
ns
D
Total N3
ns
E
Total N6
ns
F
Control T2DM 95% confidence intervals
Palmitoleic acid
Palmitic acid
Oleic acid
C14:1N5
p-value(t test)
Mean proportions (ug/mL)
Difference in mean proportions
G
Oleic acid
Palmitic acid
C14:0
Palmitoleic acid
-log10(p) = 1.301
VIP = 1
VIP
H
IL-1β
0.032
mmol/L
I
TNF-α
ns
μU/mL
J
IL-6
ns
μU/mL
K
Metabolites
Microbes
Genes
Lachnospiraceae family
Coprococcus
Dorea longicatena
Lachnospira
Roseburia
Lactobacillus ruminis

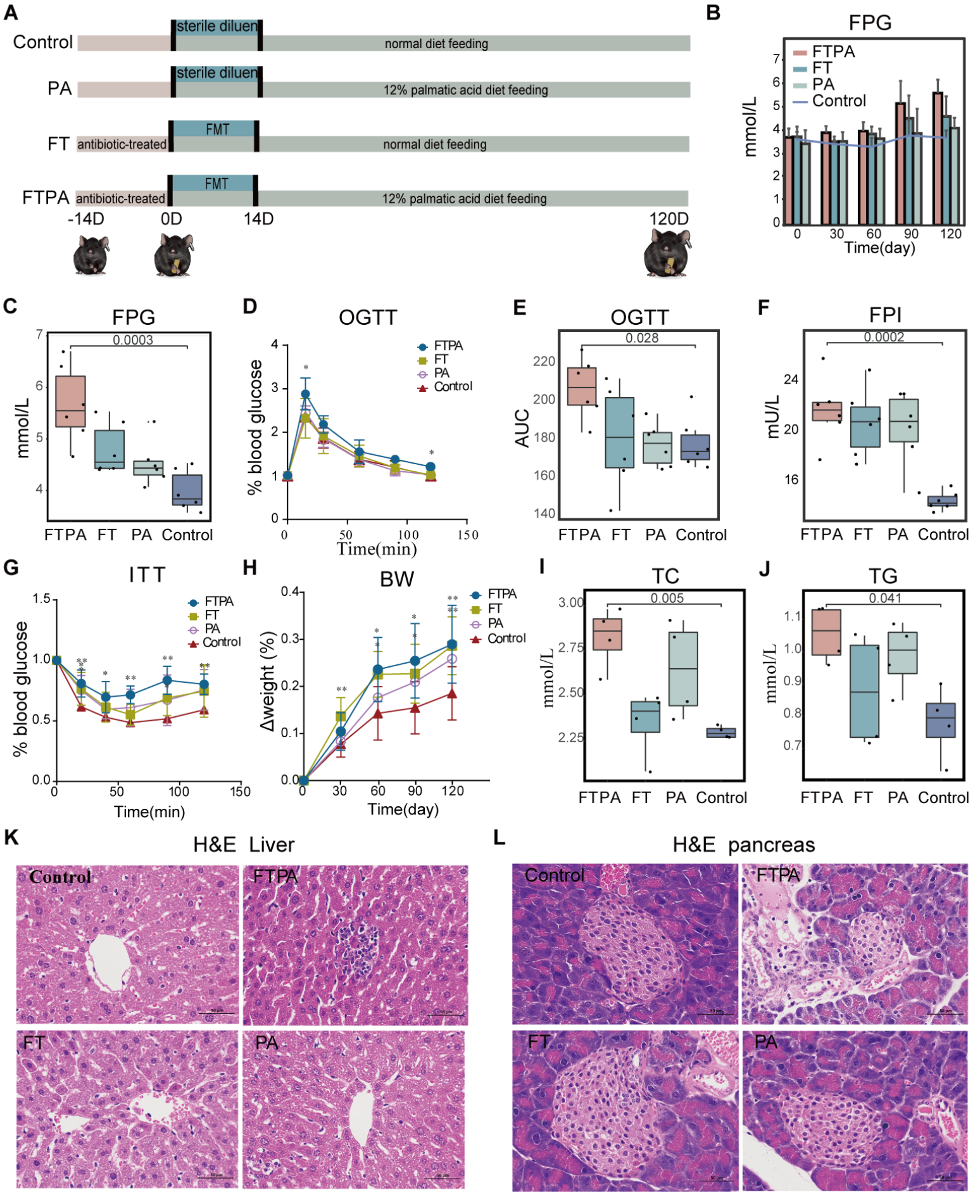
A
Control
sterile diluen
normal diet feeding
PA
sterile diluen
12% palmatic acid diet feeding
FT
antibiotic-treated
FMT
normal diet feeding
FTPA
antibiotic-treated
FMT
12% palmatic acid diet feeding
-14D
0D
14D
120D
B
FPG
FTPA
FT
PA
Control
mmol/L
Time(day)
C
FPG
0.0003
mmol/L
FTPA FT PA Control
D
OGTT
FTPA
FT
PA
Control
% blood glucose
Time(min)
E
OGTT
0.028
AUC
FTPA FT PA Control
F
FPI
0.0002
mU/L
FTPA FT PA Control
G
ITT
FTPA
FT
PA
Control
% blood glucose
Time(min)
H
BW
FTPA
FT
PA
Control
Δweight (%)
Time(day)
I
TC
0.005
mmol/L
FTPA FT PA Control
J
TG
0.041
mmol/L
FTPA FT PA Control
K
H&E Liver
Control
FTPA
FT
PA
L
H&E pancreas
Control
FTPA
FT
PA

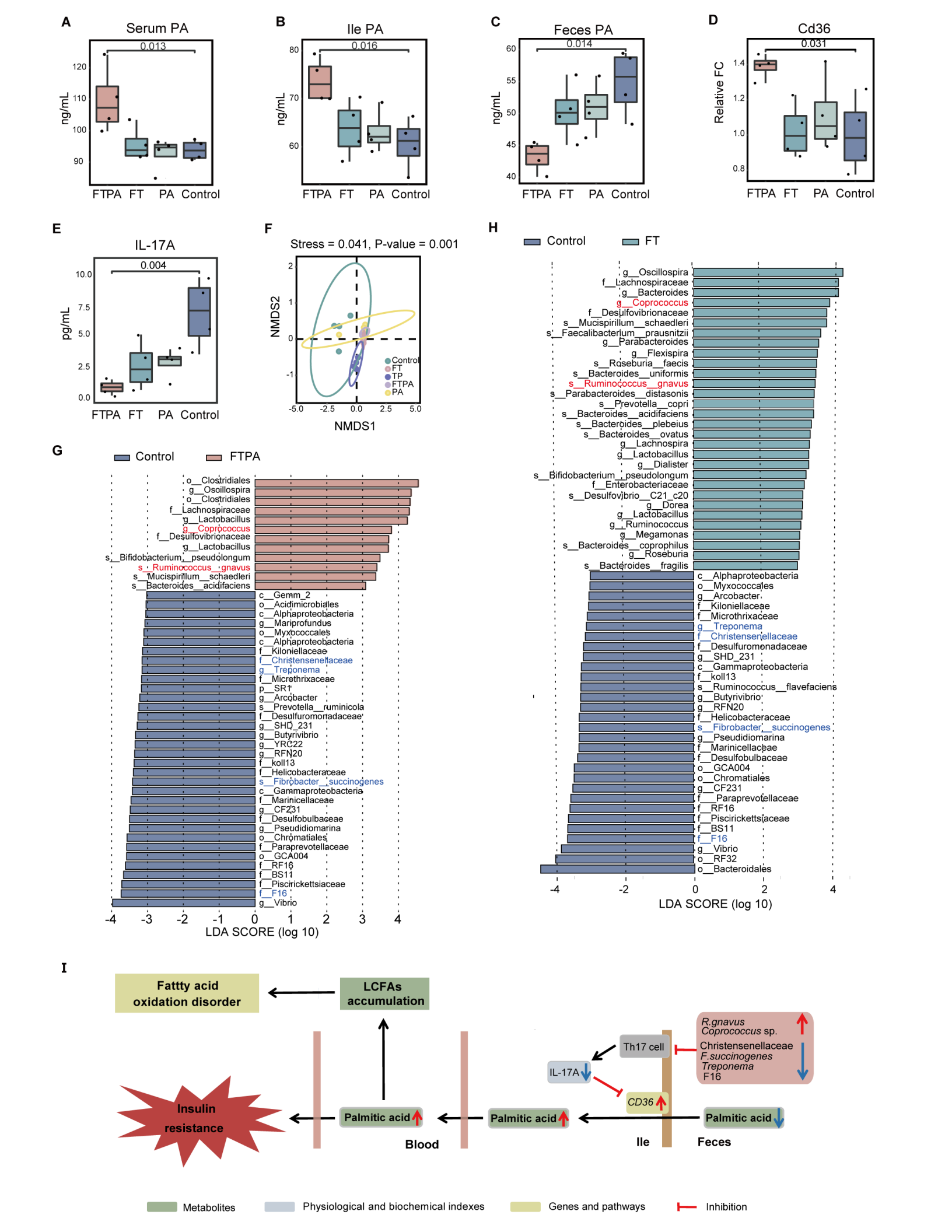
A
Serum PA
0.013
ng/mL
FTPA FT PA Control
B
Ile PA
0.016
ng/mL
FTPA FT PA Control
C
Feces PA
0.014
ng/mL
FTPA FT PA Control
D
Cd36
0.031
Relative FC
FTPA FT PA Control
E
IL-17A
0.004
pg/mL
FTPA FT PA Control
F
Stress = 0.041, P-value = 0.001
NMDS2
NMDS1
Control
FT
TP
FTPA
PA
H
Control
FT
g__Oscillospira
f__Lachnospiraceae
g__Bacteroides
g__Coprococcus
f__Desulfovibrionaceae
s__Mucispirillum__schaedleri
s__Faecalibacterium__prausnitzii
g__Parabacteroides
g__Flexispira
s__Roseburia__faecis
s__Bacteroides__uniformis
s__Ruminococcus__gnavus
s__Parabacteroides__distasonis
s__Prevotella__copri
s__Bacteroides__acidifaciens
s__Bacteroides__plebeius
s__Bacteroides__ovatus
g__Lachnospira
g__Lactobacillus
g__Dialister
s__Bifidobacterium__pseudolongum
f__Enterobacteriaceae
s__Desulfovibrio__C21_c20
g__Dorea
g__Lactobacillus
g__Ruminococcus
g__Megamonas
s__Bacteroides__coprophilus
g__Roseburia
s__Bacteroides__fragilis
c__Alphaproteobacteria
o__Myxococcales
g__Arcobacter
f__Kiloniellaceae
f__Microthrixaceae
g__Treponema
f__Christensenellaceae
f__Desulfuromonadaceae
g__SHD_231
c__Gammaproteobacteria
f__koll13
s__Ruminococcus__flavefaciens
g__Butyrivibrio
g__RFN20
f__Helicobacteraceae
s__Fibrobacter__succinogenes
g__Pseudidiomarina
f__Marinicellaceae
f__Desulfobulbaceae
o__GCA004
o__Chromatiales
g__CF231
f__Paraprevotellaceae
f__RF16
f__Piscirickettsiaceae
f__BS11
f__F16
g__Vibrio
o__RF32
o__Bacteroidales
LDA SCORE (log 10)
G
Control
FTPA
o__Clostridiales
g__Oscillospira
o__Clostridiales
f__Lachnospiraceae
g__Lactobacillus
g__Coprococcus
f__Desulfovibrionaceae
g__Lactobacillus
s__Bifidobacterium__pseudolongum
s__Ruminococcus__gnavus
s__Mucispirillum__schaedleri
s__Bacteroides__acidifaciens
c__Gemm_2
o__Acidimicrobiales
c__Alphaproteobacteria
g__Mariprofundus
o__Myxococcales
c__Alphaproteobacteria
f__Kiloniellaceae
f__Christensenellaceae
g__Treponema
f__Microthrixaceae
p__SR1
g__Arcobacter
s__Prevotella__ruminicola
f__Desulfuromonadaceae
g__SHD_231
g__Butyrivibrio
g__YRC22
g__RFN20
f__koll13
f__Helicobacteraceae
s__Fibrobacter__succinogenes
c__Gammaproteobacteria
f__Marinicellaceae
g__CF231
f__Desulfobulbaceae
g__Pseudidiomarina
o__Chromatiales
f__Paraprevotellaceae
o__GCA004
f__RF16
f__BS11
f__Piscirickettsiaceae
f__F16
g__Vibrio
LDA SCORE (log 10)
I
Fattty acid oxidation disorder
LCFAs accumulation
Insulin resistance
Palmitic acid
Blood
Palmitic acid
Ile
Palmitic acid
Feces
Th17 cell
IL-17A
CD36
R.gnavus
Coprococcus sp.
Christensenellaceae
F.succinogenes
Treponema
F16
Metabolites
Physiological and biochemical indexes
Genes and pathways
Inhibition

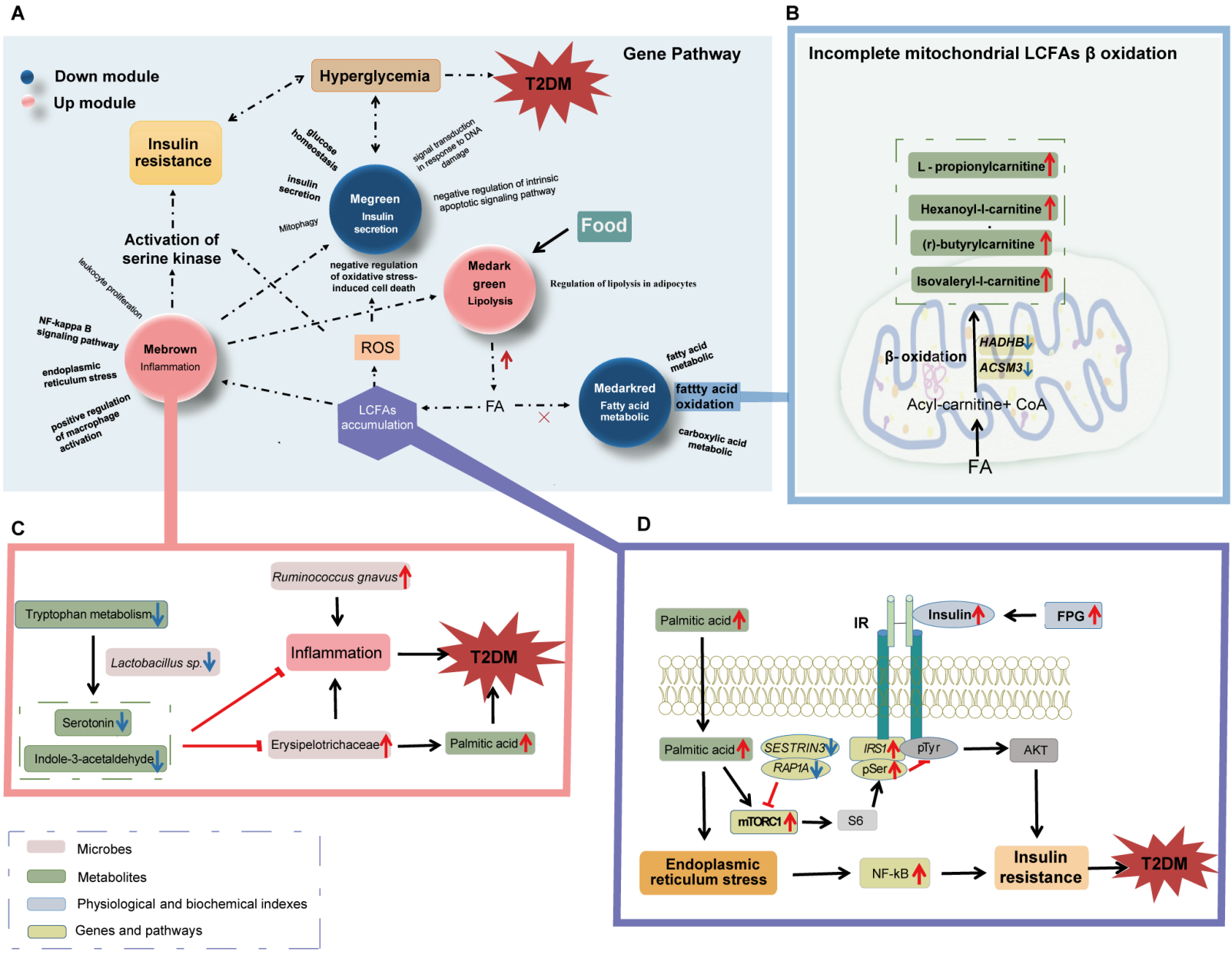
A
Down module
Up module
Gene Pathway
Hyperglycemia
T2DM
Insulin resistance
glucose homeostasis
signal transduction in response to DNA damage
insulin secretion
Megreen
Insulin secretion
negative regulation of intrinsic apoptotic signaling pathway
Mitophagy
Food
Activation of serine kinase
leukocyte proliferation
negative regulation of oxidative stress-induced cell death
Medark green
Lipolysis
Regulation of lipolysis in adipocytes
NF-kappa B signaling pathway
Mebrown
Inflammation
endoplasmic reticulum stress
ROS
positive regulation of macrophage activation
LCFAs accumulation
FA
Medarkred
Fatty acid metabolic
fatty acid metabolic
fattty acid oxidation
carboxylic acid metabolic
B
Incomplete mitochondrial LCFAs β oxidation
L - propionylcarnitine
Hexanoyl-l-carnitine
(r)-butyrylcarnitine
Isovaleryl-l-carnitine
β- oxidation
HADHB
ACSM3
Acyl-carnitine+ CoA
FA
C
Ruminococcus gnavus
Tryptophan metabolism
Lactobacillus sp.
Inflammation
T2DM
Serotonin
Indole-3-acetaldehyde
Erysipelotrichaceae
Palmitic acid
D
Palmitic acid
IR
Insulin
FPG
Palmitic acid
SESTRIN3
RAP1A
IRS1
pTyr
pSer
AKT
mTORC1
S6
Endoplasmic reticulum stress
NF-kB
Insulin resistance
T2DM
Microbes
Metabolites
Physiological and biochemical indexes
Genes and pathways